ADVANCED FUNCTIONAL MATERIALS
www.afm-journal.de

Diketopyrrolopyrrole Organic Thin-Film Transistors: Impact of Alkyl Substituents and Tolerance of Ethylhexyl Stereoisomers

Matthias Stolte, Sabin-Lucian Suraru, Patricia Diemer, Tao He, Christian Burschka, Ute Zschieschang, Hagen Klauk, and Frank Würthner**

Bis(thiophen-2-yl)-diketopyrrolopyrrole (DPP) dyes bearing various alkyl substituents at the amide positions (*n*-butyl, *n*-pentyl, *n*-hexyl, *n*-heptyl, *n*-octyl, 2-ethylhexyl) and chlorine (Cl), bromine (Br), or cyano (CN) substituents at the thiophene positions have been synthesized and investigated with regard to their molecular and semiconducting properties. Intense absorption, strong fluorescence, and reversible oxidation and reduction processes are common to all of these dyes. Their characterization as organic semiconductors in vacuum-processed thin-film transistors reveals p-channel operation with field-effect mobilities ranging from 0.01 to 0.7 cm^2 V^{-1} s^{-1}. The highest mobility is found for the DPP dyes bearing the 2-ethylhexyl substituents, which is surprising, considering that as a result of the chiral substituents, this material is a mixture of (*R*,*R*), (*S*,*S*), and (*R*,*S*) stereoisomers. The high carrier mobility in the films of the DPPs bearing stereoisomerically inhomogeneous ethylhexyl groups is rationalized here by single-crystal X-ray diffraction (XRD) analysis in combination with XRD and atomic force microscopy studies on thin films, which reveal the presence of slightly different 2D layer arrangements for the *n*-alkyl and the 2-ethylhexyl derivatives. For the cyano-substituted DPPs possessing the lowest LUMO levels, ambipolar transport characteristics are observed.

1. Introduction

Next to phthalocyanine and perylene bisimide pigments, diketopyrrolopyrroles (DPPs)[1] made the most significant impact among pigment-based organic semiconductors[2] in the field of organic electronics during the last decade. The major impact of DPPs has been in organic photovoltaics, which is likely due to their favorable combination of excellent absorption properties in the visible range and a comparably small molecule π-skeleton, which affords better solubility compared with the more extended π-scaffolds of phthalocyanine and perylene bisimide dyes. Other advantageous structural properties of DPPs are the two amide and two aromatic groups, which allow the introduction of substituents, as the former group can be functionalized with solubilizing alkyl chains[3] and the latter with substituents having certain electronic properties that can be used to tune the optical and electronic characteristics.[4] Most importantly, in particular for thiophene-derivatized DPPs, a wide variety of semiconducting polymers with alternating DPP and semiconducting oligomer subunits have been obtained that exhibit various desirable properties, such as a small bandgap, excellent charge-carrier mobilities, and suitable energy levels for bulk heterojunction solar cells with fullerene derivatives.[5]

However, these tailored semiconducting polymers can hardly be considered as DPPs anymore, due to the significant influence of the electron-donating semiconducting oligomers, which are themselves known as highly suitable π-scaffolds for organic electronics, and due to strong electronic coupling between the two constituent building blocks with their electron donor and acceptor characteristics. This ambiguity also exists for the most successful DPP-based small molecules for organic photovoltaics developed by the Nguyen group, which consist of a DPP core and two attached heterocyclic units, such as terthiophene.[6] In contrast, for the pure DPP π-scaffold, only a few studies[7] exist that provide insight into its electronic properties, the preferential solid-state packing, and the performance in organic transistors. Accordingly, after our initial communication on a cyanothienyl-substituted DPP derivative with a relatively large p-channel carrier mobility of 0.7 cm^2 V^{-1} s^{-1},[8] we report here our comprehensive studies on a broad series of 24 DPP dyes bearing thiophene substituents that were functionalized with chlorine (Cl), bromine (Br), or cyano (CN) groups to tune their electronic states and with various alkyl chains at the amide positions to direct their solid-state packing. Particular emphasis is placed on the role of racemic ethylhexyl (Ethex) substituents which were found to enable perfect terrace growth of crystalline DPP-Ethex dye layers on the gate dielectric,

Dr. M. Stolte, Dr. S.-L. Suraru, P. Diemer, Dr. T. He,
Dr. C. Burschka, Prof. F. Würthner
Institut für Organische Chemie and Center for
Nanosystems Chemistry
Universität Würzburg
Am Hubland, 97074 Würzburg, Germany
E-mail: wuerthner@chemie.uni-wuerzburg.de
Dr. U. Zschieschang, Dr. H. Klauk
Max Planck Institute for Solid State Research
Heisenbergstrasse 1, 70569 Stuttgart, Germany
E-mail: h.klauk@fkf.mpg.de

DOI: 10.1002/adfm.201602994

leading consistently to the largest carrier mobilities within each individual series of H-, Cl-, Br-, and CN-DPPs, despite their presence as "impure" mixtures of (*R*,*R*), (*S*,*S*), and (*R*,*S*) stereoisomers.[6b,7e,9]

2. Results and Discussion

2.1. Synthesis and Molecular Properties

The synthesis of the DPP dyes investigated here was accomplished in a straightforward way according to the synthetic routes depicted in **Scheme 1**. In the first step, the literature-known bis(thiophen-2-yl) DPP (Th_2-DPP) precursor was alkylated at the amide nitrogens with various bromoalkanes according to a standard procedure.[10] In the next step, the *N*-alkylated DPPs were further brominated or chlorinated at the thiophene groups with *N*-bromo- or *N*-chloro-succinimide, respectively, which are known to be suitable halogenation reagents for thiophenes with sufficient reactivity even at low temperatures.[11] The brominated thienyl-DPPs were further reacted with copper cyanide at elevated temperatures to obtain the corresponding cyano-substituted thienyl-DPP derivatives.

For the elucidation of the molecular properties of DPP dyes bearing different electron-withdrawing substituents X at the thiophene groups, we chose the *n*-octyl-substituted derivatives X-**DPP**-C_8 (X: H, Cl, Br, CN), owing to their good solubility in common solvents like dichloromethane. All these DPP derivatives show optical properties that are characteristic for the class of DPP dyes (**Figure 1** and **Table 1**). As expected, the alkyl groups (R: 2-ethylhexyl (Ethex) or C_nH_{2n+1}; *n*: 4–8) within a series of X-DPP-R dyes have no effect on the optical properties in solution (Table S1, Supporting Information). In contrast, the absorption maxima (λ_{max}) are shifted with variation of X over a narrow range from 549 nm for the parent dye H-DPP to 565 nm (Cl-DPP) and 568 nm (Br-DPP) up to 586 nm (CN-DPP), while for the molar extinction coefficients (ε_{max}), only small variations are observable (Table 1). This reduction of the optical band gap ($E_{h\nu}$) by ≈0.1 eV from H-DPP to CN-DPP is in accordance with the narrowing of the electrochemical band gap (E_{CV}), as determined by cyclic voltammetry (CV), due to the larger influence of the substituents on the reduction than on the oxidation potential (**Figure 2** and Table 1). Thus, the former increases from −1.67 V (H-DPP) versus ferrocene/ferrocenium up to −1.23 V (CN-DPP), while the latter increases only from 0.5 V (H-DPP) to 0.83 V (CN-DPP). We may accordingly conclude that the electron-withdrawing substituents have a somewhat larger influence on the LUMO level than on the HOMO level (Table 1) of the DPP scaffold and that all these dyes can still be regarded as p-channel semiconductors whose donor character is sufficiently

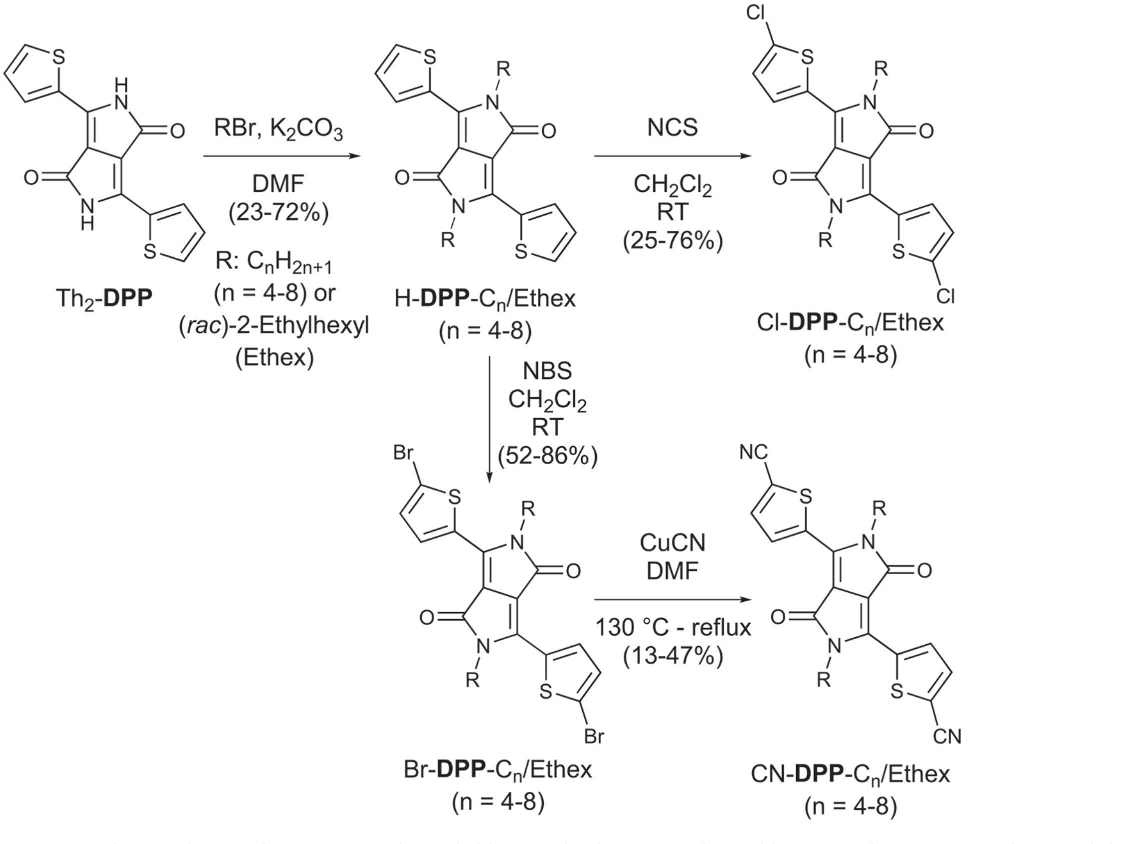

Scheme 1. Synthetic routes to the unsubstituted (H-**DPP**-C_n/Ethex), dichlorinated (Cl-**DPP**-C_n/Ethex), dibrominated (Br-**DPP**-C_n/Ethex), and dicyanated bis(thiophen-2-yl)-diketopyrrolopyrroles (CN-**DPP**-C_n/Ethex) with different solubilizing groups (R: 2-ethylhexyl (Ethex) or C_nH_{2n+1}; *n*: 4–8) at the ascribed positions.

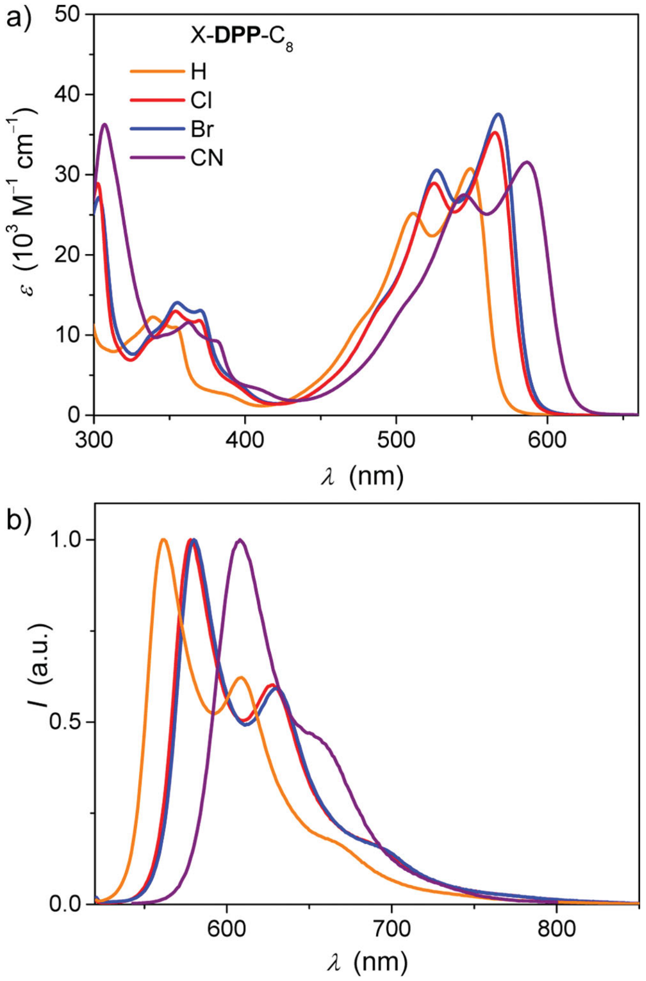

Figure 1. a) Absorption (10^{-5} M) and b) normalized emission spectra (λ_{ex} = 516 nm, <10^{-6} M) of representative DPP derivatives H-**DPP**-C_8 (orange), Cl-**DPP**-C_8 (red), Br-**DPP**-C_8 (blue), and CN-**DPP**-C_8 (violet) in CH_2Cl_2 at 298 K.

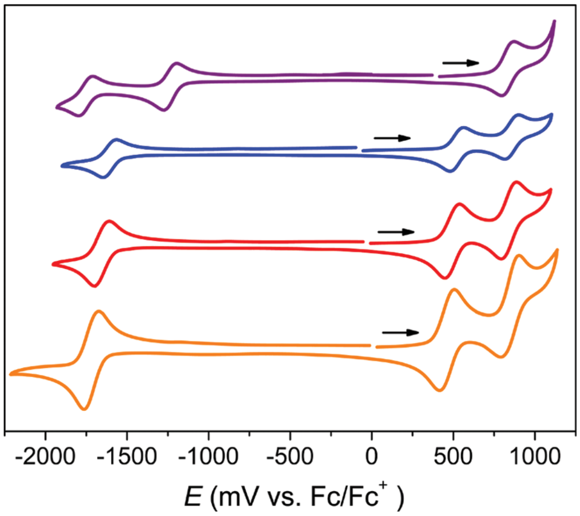

Figure 2. Cyclic voltammograms of representative DPP derivatives H-**DPP**-C_8 (orange), Cl-**DPP**-C_8 (red), Br-**DPP**-C_8 (blue), and CN-**DPP**-C_8 (violet) at a concentration of 2×10^{-4} M in CH_2Cl_2 at 298 K using ferrocene as an internal standard and NBu_4PF_6 (0.1 M) as electrolyte (scan speed: 100 mV s^{-1}).

strong to be useful for BHJ solar cells in combination with fullerene derivatives.[12]

Furthermore, these thienyl-DPP dyes are interesting fluorophores with small Stokes shifts ($\Delta\bar{\nu}_{ST}$) of only a few hundred wavenumbers (Figure 1b and Table 1). Thus, while the parent H-DPP dye is an outstanding fluorophore with a fluorescence quantum yield (Φ_{fl}) of unity, the fluorescence quantum yields of the Cl-DPP and Br-DPP derivatives are still very high (0.84 each), while that of the cyano derivative CN-DPP is slightly smaller with 0.7 (Table 1). It is interesting to note that, as in the case of other halogenated dyes,[13] no heavy-atom effect leading to triplet formation is observed for this series of dyes.

Table 1. Optical and electrochemical properties of four representative compounds X-**DPP**-C_8 (X: H, Cl, Br, CN) in CH_2Cl_2 at 298 K.

X	λ_{max} a) [nm]	ε_{max} a) [M^{-1} cm^{-1}]	E_{hv} a) [eV]	λ_{em} b) [nm]	Φ_{fl} b) [%]	$\Delta\bar{\nu}_{ST}$ [cm^{-1}]	
H	549	30 400	2.26	562	100	420	
Cl	565	35 200	2.19	578	84	400	
Br	568	37 600	2.18	580	84	365	
CN	586	31 500	2.12	609	70	645	
X	$E_{1/2}^{Red2}$ [V]	$E_{1/2}^{Red1}$ [V]	$E_{1/2}^{Ox1}$ [V]	$E_{1/2}^{Ox2}$ [V]	HOMO d) [eV]	LUMO e) [eV]	E_{CV} c) [eV]
H	–	−1.67	0.50	0.88	−5.30	−3.13	2.17
Cl	–	−1.57	0.55	0.88	−5.35	−3.23	2.12
Br	–	−1.56	0.56	0.89	−5.36	−3.24	2.12
CN	−1.75	−1.23	0.83	–	−5.63	−3.57	2.06

a) 10^{-5} M; b) 10^{-6} M; c) 2×10^{-4} M; d) HOMO = −4.8 eV − $E_{1/2}^{Ox1}$; e) LUMO = −4.8 eV − $E_{1/2}^{Red1}$.

2.2. Charge-Carrier Mobility

To investigate the charge-transport properties of the thienyl-DPPs, bottom-gate, top-contact thin-film transistors (TFTs) were fabricated and characterized in air. The TFTs were fabricated on doped silicon substrates with a gate dielectric composed of 100 nm thick thermally grown SiO_2, 8 nm thick atomic-layer-deposited Al_2O_3 and either a fluoroalkyl- or an alkylphosphonic acid self-assembled monolayer (SAM, see Figure S1, Supporting Information).[14] Semiconductor layers with a thickness of 30 nm were deposited by thermal sublimation in vacuum at an elevated substrate temperature (T_S) to obtain crystalline semiconductor layers. Au source and drain contacts were deposited onto the organic semiconductor using a shadow mask.

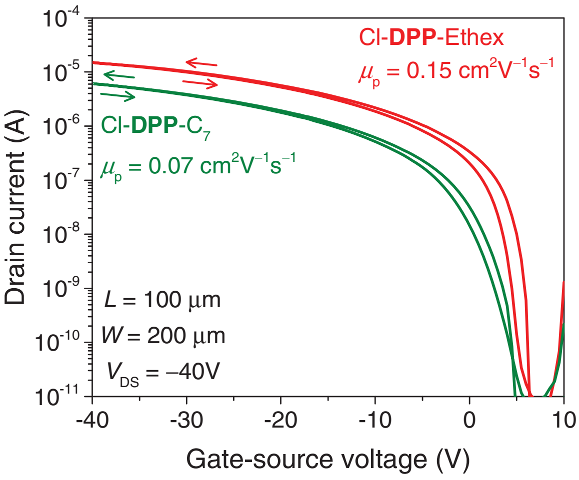

Figure 3. Transfer characteristics of TFTs based on vacuum-deposited layers of Cl-**DPP**-Ethex (red) and Cl-**DPP**-C$_7$ (green) measured in ambient air.

The TFTs exhibit p-channel operation with hole mobilities (μ_p) ranging from 0.01 to 0.7 cm^2 V^{-1} s^{-1}, on/off ratios (I_{on}/I_{off}) between 10^5 and 10^7, and threshold voltages (V_T) between −4 and +9 V for the H/Cl/Br-DPPs and between −14 and −27 V for the electron-deficient CN-DPPs (see **Figure 3** and Table S2, Supporting Information). The observed p-channel behavior was expected for these DPP dyes, since their HOMO energy levels are close to the Fermi level of the gold contacts. The linearly alkylated electron-poor CN-DPPs display ambipolar behavior, with electron mobilities (μ_e) ranging from 0.005 to 0.04 cm^2 V^{-1} s^{-1} (see Figure S2 and Table S3, Supporting Information).

Figure 4 illustrates the influence of the substituents at the thiophene and amide positions on the hole mobility. As can be seen, the hole mobilities of the Cl- and Br-DPPs are all very similar (between 0.05 and 0.15 cm^2 V^{-1} s^{-1}) and notably larger than those of the parent dye H-DPPs (between 0.01 and 0.09 cm^2 V^{-1} s^{-1}).

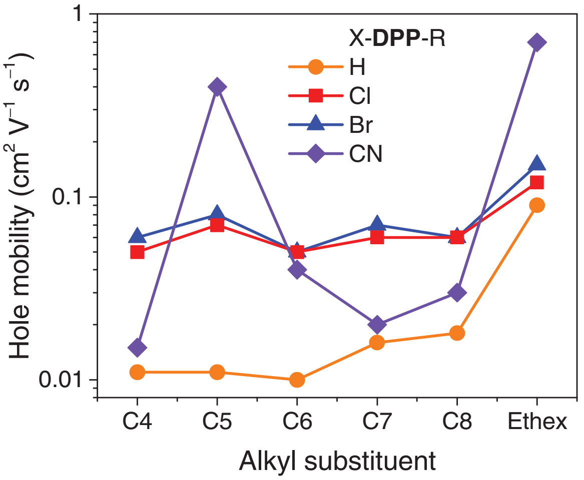

Figure 4. Influence of the substituents at the thiophene positions (H: orange, Cl: red, Br: blue, CN: violet) and at the amide positions (*n*-butyl, *n*-pentyl, *n*-hexyl, *n*-heptyl, *n*-octyl, 2-ethylhexyl) on the hole mobility of the TFTs with fluoroalkylphosphonic acid SAM (see also Table S2, Supporting Information). Average value of five transistors, which showed a variation of less than 10%.

Most interestingly, the largest hole mobilities for each series were obtained for the 2-ethylhexyl-substituted DPPs (H-**DPP**-Ethex: 0.09 cm^2 V^{-1} s^{-1}; Cl-**DPP**-Ethex: 0.15 cm^2 V^{-1} s^{-1}; Br-**DPP**-Ethex: 0.12 cm^2 V^{-1} s^{-1}; CN-**DPP**-Ethex: 0.7 cm^2 V^{-1} s^{-1}), while the mobilities of the DPPs with linear alkyl chains in each series show – with exception of the CN-DPPs – only a weak dependence on the alkyl chain length (0.01 to 0.03 cm^2 V^{-1} s^{-1} for the H-DPPs; 0.05 to 0.08 cm^2 V^{-1} s^{-1} for the Cl-DPPs (Figure S3, Supporting Information); 0.05 to 0.07 cm^2 V^{-1} s^{-1} for the Br-DPPs; 0.01 to 0.4 cm^2 V^{-1} s^{-1} for the CN-DPPs). The largest mobility of 0.7 cm^2 V^{-1} s^{-1} among the complete series of DPP dyes was obtained for CN-**DPP**-Ethex. This remarkable result seems at first glance rather puzzling, as one would expect that the packing of the branched, racemic 2-ethylhexyl-substituted dyes in thin films should be rather unfavorable and inhomogeneous by the presence of (*R*,*R*), (*S*,*S*), and (*R*,*S*/*S*,*R*) stereoisomers. However, using chiral high perforamce liquid chromatography analysis we have been able to verify that for all X-**DPP**-Ethex compounds the mesomer (*R*,*S*) is considerably enriched by the last purification step, i.e., by the recrystallization, so that only minor fractions of about 20% of the enantiomers (*R*,*R*) and (*S*,*S*) remain in each batch (Figure S4, Supporting Information). A second notable outcome of our study is that the length of the *n*-alkyl chain has almost no influence on the TFT performance. In particular, no (H- and CN-DPPs) or only a very small odd–even effect (Cl- and Br-DPPs) is observed, which suggests that all DPP molecules bearing *n*-alkyl chains are deposited in a similar arrangement on the fluorinated gate dielectric.

2.3. Supramolecular Ordering and Morphology

To shed light onto the rather unexpected finding that the DPP dyes with the branched, chiral alkyl chains produce the largest carrier mobilities, we will discuss in the following the structural features of these DPP molecules that determine the TFT performance, starting with (I) molecular geometry, followed by (II) molecular packing in the solid state, and finally (III) macroscopic thin-film morphology of three representative compounds with linear and branched alkyl chains having the same thiophene substituent X = Cl.

To obtain insight into the preferential arrangement of the molecules in the solid state and gain a better understanding of the consequences on the charge transport, we attempted to grow single crystals suitable for X-ray analysis. We succeeded for Cl-**DPP**-C$_7$, Cl-**DPP**-C$_8$, and the mesomer (*R*,*S*/*S*,*R*) of Cl-**DPP**-Ethex by slow diffusion of an unpolar solvent into a highly concentrated solution of each molecule dissolved in solvents of higher polarity. The obtained single-crystal structures were analyzed at a temperature of 300 K (**Figure 5**; Table S4 and Figure S5, Supporting Information). It is important to note that Cl-**DPP**-C$_7$ and Cl-**DPP**-C$_8$ exhibit almost identical packing arrangements (Figure S5, Supporting Information). Thus, with $a \approx 4.83$ Å and $b \approx 8.7$ Å the *a*,*b*-plane is almost identical, whereas the third parameter of the unit cell (*c*) changes to accommodate the particular alkyl chain length. In addition,

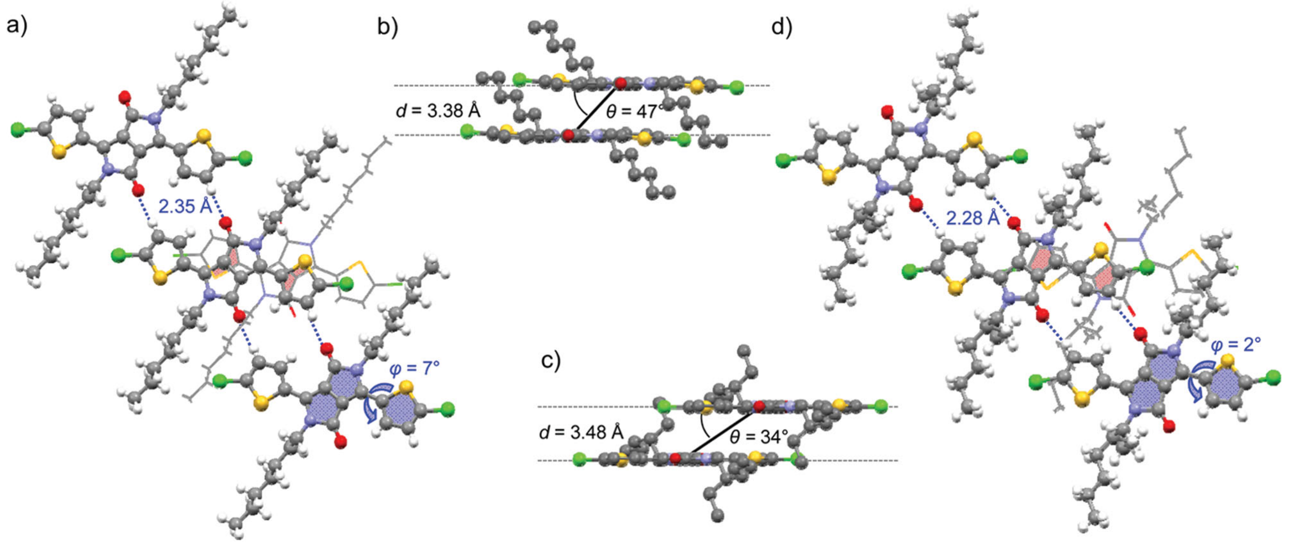

Figure 5. Top view (a,d) onto the hydrogen-bonded network and side view (b,c) onto two π-stacked molecules of Cl-**DPP**-C_7 (a,b) and Cl-**DPP**-Ethex(*R*,*S*) (c,d). a,d) The distances between lactam carbonyl and the thiophene hydrogen (C=O…H) of neighboring molecules, the torsion angle ϕ between DPP core and the thiophenes are given in blue, while the minimal overlap of the π-system is indicated as red area. b,c) Their average π–π distance (*d* [Å]) and the longitudinal displacement of the DPP centers θ are indicated.

we confirmed the identical packing of the molecules in the thin films by X-ray diffraction (XRD, **Figure 6**a) analysis to correlate the in-plane distances with the lattice parameters of the unit cell of the single crystals and with the heights of the molecular terraces determined by atomic force microscopy (AFM, Figure 6b; Figure S6, Supporting Information). Most interestingly and in accordance with the large carrier mobilities of the DPP-Ethex dyes (Figure 4), the 20% content of (*R*,*R*) and (*S*,*S*) enantiomers within the batch of Cl-**DPP**-Ethex did not prevent the highly crystalline solid-state packing, and indeed the arrangement of the molecules was found to be almost identical in the single-crystal of the mesomer (*R,S*) and in the thin-film.

On the molecular level (I) the three crystal structures reveal almost identical π-scaffolds for the DPP units whose C—C, C—N, and C—O bond lengths are in accordance with a delocalized and fully conjugated π-system. The only evident difference between the molecules with linear (Cl-**DPP**-C_7, Cl-**DPP**-C_8) and branched alkyl chains (Cl-**DPP**-Ethex (*R,S*) mesomer) is in the torsion angle ϕ between the DPP core and the two thiophene substituents. While for the latter the entire π-system is almost

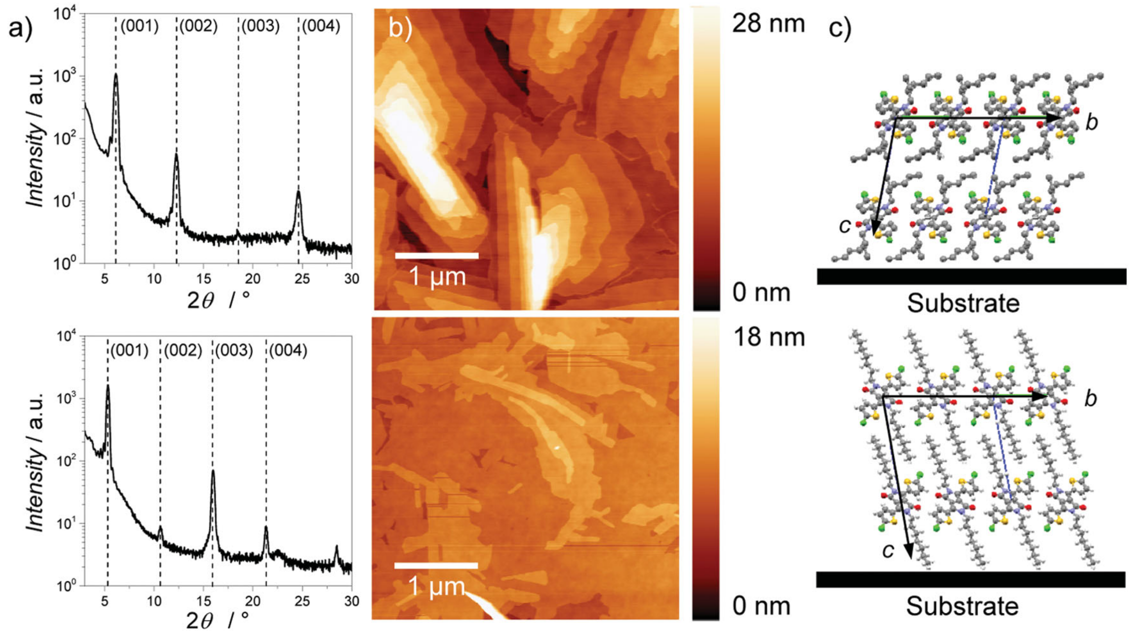

Figure 6. a) XRD with indexed (00i) reflexes of vacuum-deposited layers of OTFTs of Cl-**DPP**-Ethex (top) and Cl-**DPP**-C_7 (bottom), b) respective AFM images, c) as well as orientation of the molecules with respect to the substrate determined by XRD (view along *a*-axis).

planar ($\phi \approx 2°$), ϕ increases considerably for Cl-**DPP**-C_7 and Cl-**DPP**-C_8 up to 7°, representing a slight distortion of the dyes' π-scaffold (Figure 5). This difference is obviously caused by the optimization of the molecular packing (II) within the single-crystals as well as in the thin films of the respective dyes. While the molecular interactions in the solid state for all of these DPPs are based on (a) π–π-stacking of the DPP units, (b) segregation of the DPP cores and the alkyl side chains, and (c) hydrogen-bonding between the lactam carbonyl group and the protons of the thiophenes, one can observe significant differences. For the almost planar Cl-**DPP**-Ethex (*R,S*) mesomer all H-bonded molecules lie in close proximity in one plane (2.28 Å). In contrast the twist of $\phi \approx 7°$ causes a staircase-like arrangement of the molecules Cl-**DPP**-C_7 and Cl-**DPP**-C_8 with slightly larger H-bonds of 2.35 Å (Figure 5a,d; Figure S5, Supporting Information). Additionally, while the linear alkyl chains of molecules of different layers interdigitate, the sterical bulkiness of the branched 2-ethylhexyl groups prohibits such an arrangement and causes the segregation of the individual layers along the *c*-axis (Figures 5 and 6c). Concomitantly, the π–π-distance between neighbouring molecules increases slightly from 3.38 Å (Cl-DPP-C_7, Cl-**DPP**-C_8) to 3.48 Å (Cl-**DPP**-Ethex(*R,S*)), and the lateral shift of the DPP center is increased, giving rise to a reduction of the slip angle from $\theta = 47°$ (Cl-**DPP**-C_7, Cl-**DPP**-C_8) to $\theta = 34°$ (Cl-**DPP**-Ethex(*R,S*), see Figure 5b,c). The reduced slip appears to have a beneficial impact on the charge transport for the DPP with branched alkyl chains, as it enables a larger overlap between the DPP core and the thiophene units of neighbouring molecules (red areas in Figure 5a,d). Likewise, the closer hydrogen-bond-connected assembly of DPP-Ethex molecules in one plane might be considered beneficial, while the increase in distance will obviously act adversely. We have also carried out calculations of charge-transfer integrals for the respective DPP dye arrangements (π-stacked and hydrogen-bonded) of Cl-**DPP**-Ethex(*R,S*) and Cl-**DPP**-C_7 crystals (see Table S5, Supporting Information). However, the values are quite similar for the two derivatives and thus cannot be used to rationalize the consistently larger charge-carrier mobilities observed in the ethylhexyl derivatives.

Finally, on the macroscopic level (III) the thin films display a layer-like growth with domain sizes on the order of several 10 μm^2 (Figure 6b). The step heights of these layers determined by AFM (1.7 nm for Cl-**DPP**-C_7; 1.5 nm for Cl-**DPP**-Ethex, Figure S7, Supporting Information) are in good agreement with the length of the *c*-axis of the respective unit cells (1.71 nm, 1.49 nm). This assignment is confirmed by the XRD measurements, which show multiple diffraction peaks at precisely the 2θ values expected from the single-crystal structures (Figure 6a), even for the mixture of the Cl-**DPP**-Ethex stereoisomers. From the assignment of the (001) diffractions we can determine an edge-on orientation of the molecules with respect to the substrate plane, as visualized in Figure 6c. It is therefore reasonable to rationalize the charge-carrier mobilities of the X-DPP derivatives bearing linear alkyl chains (Figure 4) by their similar packing arrangement which provides essentially identical 2D DPP layers irrespective of the alkyl chain length (Figure 6c). Upon introduction of the branched Ethex chain, however, such an arrangement with interdigitated alkyl chains is not possible, due to the greater sterical demands which direct the DPP molecules into even more beneficial 2D layers with all DPP cores in one plane and improved π–π-contacts between the layers. In addition, the layer heights between the Cl-**DPP**-Ethex molecules are reduced by about 2.1 Å compared to those between the Cl-**DPP**-C_7 and Cl-**DPP**-C_8 molecules, and more regularly shaped domains and terrace-like growth are observed (Figure 6b). All these facts possibly favor the efficiency of the injection (and extraction) of charges from the source contact into the semiconductor (and from the semiconductor into the drain contact) and possibly enable more efficient percolation pathways within the domains of the Cl-**DPP**-Ethex thin films. An additional factor that limits the carrier mobility in TFTs based on polycrystalline semiconductors is the efficiency of the charge transport across the grain boundaries in the carrier channel, but since this channel is located at the interface to the gate dielectric, it is not accessible by AFM.

Interestingly, highly crystalline layers of Cl-**DPP**-Ethex molecules with a packing behavior identical to the single-crystal structure of the (*R,S*) mesomer are obtained by vacuum deposition of a mixture of the enantiomers (*R,R*), (*S,S*), and the (*R,S*) mesomer (ratio about 10:10:80, see Figure S4, Supporting Information). It is generally assumed that such a mixture of molecules cannot co-assemble into a crystalline lattice. However, in a recent article Percec and co-workers described a similar phenomenon for perylene bisimides. They showed that identical single-crystal-like order can originate from both homochiral and racemic perylene bisimide compounds and even from mixtures of diastereomers that cannot give single-handed helical assemblies, disregarding the chirality of the self-assembling building blocks.[15] Our ongoing studies are aimed at establishing a better understanding of this intriguing phenomenon and its impact on charge carrier transport for X-**DPP**-Ethex molecules in single crystal transistor devices.

3. Conclusion

In this article we have investigated the influence of halogen and cyano substituents on the optical and electronic properties of DPP dyes and shown that these substituents are ideally suited to tune the dyes' absorption and redox properties into a favorable regime for applications in organic transistors and solar cells. Furthermore, we could show by a variation of alkyl groups at the amide nitrogens distinct differences in OTFT performance between derivatives with linear and branched side chains that could be rationalized by different packing arrangements derived from single-crystal structure analysis. Accordingly, DPPs substituted with linear alkyl chains grow in layers with interdigitated alkyl chains along the substrate normal. On the other hand, to accommodate the more bulky branched Ethex chain a slightly different packing of the DPP core is enforced, leading to superior π–π-contacts between DPP molecules within the layers and closer distances between the DPP layers which are both favorable for charge-carrier transport. Most remarkably, and of great value for applications of DPP molecules in devices, by far the best p-channel transistors could be obtained for vacuum-processed devices with Ethex-functionalization despite the presence of stereoisomeric mixtures of 2-ethylhexyl substituents for all series of chlorinated, brominated, and cyanated dyes. This remarkable result suggests that the packing of these dyes in thin films is not particularly disturbed by the presence of (*R*,*R*) and (*S*,*S*) enantiomers for (*R*,*S*) stereoisomer enriched samples which was confirmed by AFM and X-ray analyses. Mixtures of stereoisomers originating from racemic branched alkyl chains are accordingly not only helpful to accomplish better solubility as required for chromatographic purification and solution-processing purposes but may even enable highly crystalline layers with suitable packing arrangements as required for high-performance transistor devices.

4. Experimental Section

Materials and Methods: All reagents and solvents were obtained from commercial suppliers and purified or dried according to standard procedures. Column chromatography was performed on silica gel (Merck Silica 60, particle size 0.040–0.063 mm). Solvents for spectroscopic studies were of spectroscopic grade and used as received.

Synthesis: The synthesis of CN-**DPP**-Ethex has been reported previously[8] and the detailed synthetic procedures for the new compounds, along with their characterization by NMR and UV–vis spectroscopy, mass spectrometry, in some cases elemental analysis, and cyclic voltammetry, can be found in the Supporting Information.

Measurements and Characterization: Elemental analysis was performed on a CHNS 932 analyzer (Leco Instruments GmbH, Mönchengladbach, Germany). ^{1}H and ^{13}C spectra were recorded in $CDCl_3$ on a Bruker Advance 400 spectrometer. Residual undeuterated solvent was used as internal standard (5.32 ppm for ^{1}H, 53.84 ppm for ^{13}C). High-resolution electrospay ionization time-of-flight (ESI-TOF) mass spectrometry was carried out on a micrOTOF focus instrument (Bruker Daltronik GmbH). UV–vis measurements were performed in CH_2Cl_2 (10^{-5} M) in a conventional quartz cell (light pass 10 mm) on a Perkin–Elmer Lambda 950 or Lambda 35 spectrometer. Fluorescence spectra were recorded with a PTI QM-4/2003 instrument under ambient conditions corrected for the photomultiplier tube type R928P and lamp intensity. The fluorescence quantum yields were determined by optical dilution method (Abs < 0.05) using *N*,*N′*-di(2,6-diisopropylphenyl)-1,6,7,12-tetraphenoxy-perylene-3,4,9,10-tetracarboxylic acid bisimide ($\Phi_{\text{fl}} = 0.96\%$ in $CHCl_3$) as reference.[16] For cyclic voltammetry, a standard commercial electrochemical analyzer (EC epsilon; BAS Instruments, UK) with a three electrode single-compartment cell was used. CH_2Cl_2 (HPLC grade) was dried over calcium hydride under argon and degassed before use. The supporting electrolyte tetrabutylammonium hexafluorophosphate (NBu_4PF_6; 0.1 M) was prepared according to the literature,[17] and recrystallized from ethanol/water. The measurements were carried out in dichloromethane at a concentration of about 2×10^{-4} M with ferrocene (Fc) as an internal standard for the calibration of the potential (scan speed: 100 mV s^{-1}). Ag/AgCl, a Pt disc, and a Pt wire were used as reference, working, and auxiliary electrodes, respectively.

The single-crystal X-ray data were collected at 300 K with a Bruker X8APEX-II_KAPPA diffractometer with APEX CCD area detector and graphite monochromated $Mo_{K\alpha}$ radiation or a Bruker D8Quest Kappa Diffractometer using $Cu_{K\alpha}$ radiation from an Incoatec IμS microsource with Montel multilayered mirror, a Photon100 CMOS detector and Apex2* software. The structures were solved using direct methods, refined with SHELX software package and expanded using Fourier techniques.[18] All nonhydrogen atoms were refined anisotropically. Hydrogen atoms were assigned idealized positions and were included in structure factors calculations.

CCDC 1484923–1484925 contains the supplementary crystallographic data for this paper. These data can be obtained free of charge from The Cambridge Crystallographic Data Centre via www.ccdc.cam.ac.uk/data_request/cif.

OTFT Fabrication and Characterization: Organic TFTs were fabricated on heavily doped silicon that serves both as the substrate and as the gate electrode of the transistors. The gate dielectric consists of a 100 nm thick layer of thermally grown SiO_2, an 8 nm thick layer of Al_2O_3 (grown by atomic layer deposition), and a SAM of either 12,12,13,13,14,14,15,15,16,16,17,17,18,18,18-pentadecylfluorooctadecylphosphonic acid (kindly provided by Matthias Schlörholz) or *n*-tetradecylphosphonic acid (Alfa Aesar). A 30 nm thick layer of the organic semiconductor was deposited by thermal sublimation in vacuum. During the deposition of the organic semiconductor, the substrate was held at an elevated temperature to promote molecular ordering. Finally, Au source and drain contacts were deposited by thermal evaporation in vacuum through a shadow mask. All TFTs have a channel length of 100 μm and a channel width of 200 μm. The current–voltage characteristics were measured in ambient air at room temperature. The AFM images were processed with WSXM, a freeware scanning probe microscopy software.[19] XRD data of thin films were collected at room temperature on a Bruker D8 Discover Diffractometer with a LynxEye-1D-Detector using $Cu_{K\alpha}$ radiation (mean wavelength $\lambda = 154.19$ pm).

Supporting Information

Supporting Information is available from the Wiley Online Library or from the author.

Acknowledgements

Financial support of this work from the Ministry of education and research (BMBF) within the project POLYTOS (FKZ: 13N10205) is gratefully acknowledged.

Received: June 16, 2016
Revised: August 11, 2016

---

[1] a) Z. Hao, A. Iqbal, *Chem. Soc. Rev.* **1997**, *26*, 203; b) M. Grzybowski, D. T. Gryko, *Adv. Opt. Mater.* **2015**, *3*, 280.

[2] a) X. Gao, Y. Hu, *J. Mater. Chem. C* **2014**, *2*, 3099; b) M. Gsänger, D. Bialas, L. Huang, M. Stolte, F. Würthner, *Adv. Mater.* **2016**, *28*, 3615.

[3] M. Kirkus, L. Wang, S. Mothy, D. Beljonne, J. Cornil, R. A. J. Janssen, C. J. Meskers, *J. Phys. Chem. A* **2012**, *116*, 7927.

[4] H. Bürckstümmer, A. Weissenstein, D. Bialas, F. Würthner, *J. Org. Chem.* **2011**, *76*, 2426.

[5] a) T. L. Nelson, T. M. Young, J. Liu, S. P. Mishra, J. A. Belot, C. L. Balliet, A. E. Javier, T. Kowalewski, R. D. McCullough, *Adv. Mater.* **2010**, *22*, 4617; b) Y. Li, S. P. Singh, P. Sonar, *Adv. Mater.* **2010**, *22*, 4862; c) C. H. Woo, P. M. Beaujuge, T. W. Holcombe, O. P. Lee, J. M. J. Fréchet, *J. Am. Chem. Soc.* **2010**, *132*, 15547; d) S. Cho, J. Lee, M. Tong, J. H. Seo, C. Yang, *Adv. Funct. Mater.* **2011**, *21*, 1910; e) Y. Li, P. Sonar, S. P. Singh, M. S. Soh, M. van Meurs, J. Tan, *J. Am. Chem. Soc.* **2011**, *133*, 2198; f) P. Sonar, S. P. Singh, Y. Li, Z.-E. Ooi, T.-J. Ha, I. Wong, M. S. Soh, A. Dodabalapur, *Energy Environ. Sci.* **2011**, *4*, 2288; g) A. R. Mohebbi, J. Yuen, J. Fan, C. Munoz, M. F. Wang, R. S. Shirazi, J. Seifter, F. Wudl, *Adv. Mater.* **2011**, *23*, 4644; h) A. T. Yiu, P. M. Beaujuge, O. P. Lee, C. H. Woo, M. F. Toney, J. M. J. Fréchet, *J. Am. Chem. Soc.* **2012**, *134*, 2180; i) I. Kang, H.-J. Yun, D. S. Chung, S.-K. Kwon, Y.-H. Kim, *J. Am. Chem. Soc.* **2013**, *135*, 14896; j) J. Lee, A.-R. Han, H. Yu, T. J. Shin, C. Yang, J. H. Oh, *J. Am. Chem. Soc.* **2013**, *135*, 9540.

[6] a) B. Walker, A. B. Tamayo, X.-D. Dang, P. Zalar, J. H. Seo, A. Garcia, M. Tantiwiwat, T.-Q. Nguyen, *Adv. Funct. Mater.* **2009**, *19*, 3063; b) Y. Zhang, C. Kim, J. Lin, T.-Q. Nguyen, *Adv. Funct. Mater.* **2012**, *22*, 97.

[7] a) H. Yanagisawa, J. Mizuguchi, S. Aramaki, Y. Sakai, *Jpn. J. Appl. Phys.* **2008**, *47*, 4728; b) E. D. Głowacki, H. Coskun, M. A. Blood-Forsythe, U. Monkowius, L. Leonat, M. Grzybowski, D. Gryko, M. S. White, A. Aspuru-Guzik, N. S. Sariciftci, *Org. Electron.* **2014**, *15*, 3521; c) J. Kwon, H. Na, A. K. Palai, A. Kumar, U. Jeong, S. Cho, S. Pyo, *Synth. Met.* **2015**, *209*, 240; d) B. Sambathkumar, P. S. V. Kumar, K. Saurav, S. S. K. Iyer, V. Subramanian, N. Somanathan, *New J. Chem.* **2016**, *40*, 3803; e) Y. Qiao, Y. Guo, C. Yu, F. Zhang, W. Xu, Y. Liu, D. Zhu, *J. Am. Chem. Soc.* **2012**, *134*, 4084.

[8] S.-L. Suraru, U. Zschieschang, H. Klauk, F. Würthner, *Chem. Commun.* **2011**, *47*, 1767.

[9] a) Y. Lin, P. Cheng, Y. Lia, X. Zhan, *Chem. Commun.* **2012**, *48*, 4773; b) J. Mei, K. R. Graham, R. Stalder, J. R. Reynolds, *Org. Lett.* **2010**, *12*, 660; c) K. R. Graham, P. M. Wieruszewski, R. Stalder, M. J. Hartel, J. Mei, F. So, J. R. Reynolds, *Adv. Funct. Mater.* **2012**, *22*, 4801; d) J. Liu, Y. Zhang, H. Phan, A. Sharenko, P. Moonsin, B. Walker, V. Promarak, T.-Q. Nguyen, *Adv. Mater.* **2013**, *25*, 3645; e) J. Liu, B. Walker, A. Tamayo, Y. Zhang, T.-Q. Nguyen, *Adv. Funct. Mater.* **2013**, *23*, 47.

[10] L. Huo, J. Hou, H.-Y. Chen, S. Zhang, Y. Jiang, T. L. Chen, Y. Yang, *Macromolecules* **2009**, *42*, 6564.

[11] P. Bäuerle, F. Würthner, G. Götz, F. Effenberger, *Synthesis* **1993**, 1099.

[12] I. Seguy, P. Jolinat, P. Destrule, R. Mamy, H. Allouchi, C. Couseille, M. Cotrait, H. Bock, *ChemPhysChem* **2001**, *2*, 448.

[13] U. Mayerhöffer, B. Fimmel, F. Würthner, *Angew. Chem.* **2012**, *124*, 168; *Angew. Chem. Int. Ed.* **2012**, *51*, 164.

[14] a) R. Hofmockel, U. Zschieschang, U. Kraft, R. Rödel, N. H. Hansen, M. Stolte, F. Würthner, K. Takimiya, K. Kern, J. Pflaum, H. Klauk, *Org. Electron.* **2013**, *14*, 3213; b) U. Kraft, M. Sejfic, M. J. Kang, K. Takimiya, T. Zaki, F. Letzkus, J. N. Burghartz, E. Weber, H. Klauk, *Adv. Mater.* **2015**, *27*, 207.

[15] C. Roche, H.-J. Sun, P. Leowanawat, F. Araoka, B. E. Partridge, M. Peterca, D. A. Wilson, M. E. Prendergast, P. A. Heiney, R. Graf, H. W. Spiess, X. Zeng, G. Ungar, V. Percec, *Nat. Chem.* **2016**, *8*, 80.

[16] R. Gvishi, R. Reisfeld, Z. Burshtein, *Chem. Phys. Lett.* **1993**, *213*, 138.

[17] D. D. Perrin, W. L. Armarego, D. R. Perrin, *Purification of Laboratory Chemicals*, 2nd ed., Pergamon Press Ltd., Oxford, UK **1980**.

[18] G. M. Sheldrick, *Acta Crystallogr., Sect. A: Found. Crystallogr.* **2008**, *A64*, 112.

[19] I. Horcas, R. Fernandez, J. M. Gomez-Rodriguez, J. Colchero, J. Gomez-Herrero, A. M. Baro, *Rev. Sci. Instrum.* **2007**, *78*, 013705.

Supporting Information

Diketopyrrolopyrrole Organic Thin-Film Transistors: Impact of Alkyl Substituents and Tolerance of Ethylhexyl Stereoisomers

Matthias Stolte,[a] *Sabin-Lucian Suraru,*[a] *Patricia Diemer,*[a] *Tao He,*[a] *Christian Burschka,*[a] *Ute Zschieschang,*[b] *Hagen Klauk,**[b] *and Frank Würthner**[a]

[a] Universität Würzburg, Institut für Organische Chemie and Center for Nanosystems Chemistry, Am Hubland, 97074 Würzburg, Germany.
E-mail: wuerthner@chemie.uni-wuerzburg.de; Fax: +49 931 3184756; Tel: +49 931 3185340;

[b] Max Planck Institute for Solid State Research, Heisenbergstrasse 1, 70569 Stuttgart, Germany.
E-mail: H.Klauk@fkf.mpg.de; Fax: +49 711 6891472; Tel: +49 711 689-1401

Table of contents

1. Synthesis and Characterization S2
2. TFT Measurements S17
3. HPLC Analysis S20
4. X-ray Crystallography S21
5. Calculations of the transfer integrals S23
6. AFM Measurements S24
7. Additional References S25

1. Synthesis and Characterization

General procedure for the alkylation of Th_2-DPP:

3,6-Bis(thiophen-2-yl)pyrrolo[3,4-*c*]pyrrole-1,4(2*H*, 5*H*)-dione (Th_2-DPP, 1 equiv.) and potassium carbonate (4 equiv.) were placed in a round-bottomed flask under argon. Dry DMF and the respective *n*-alkyl bromide (4 equiv.) were added and the reaction mixture was refluxed for the specified time period before it was allowed to cool down to room temperature. The solvent was removed under reduced pressure and the residual crude product was purified by column chromatography, recrystallized from cyclohexane and dried under vacuum.

2,5-Bis(*n*-butyl)-3,6-bis(thiophen-2-yl)-pyrrolo[3,4-*c*]pyrrole-1,4-dione (H-**DPP**-C_4)[S1]

According to the general procedure Th_2-DPP (150 mg, 0.497 mmol), potassium carbonate (274 mg, 2.00 mmol) and *n*-butyl bromide (0.21 mL, 0.27 mg, 2.0 mmol) were reacted in DMF (11 mL) for 18 h. Column chromatography (dichloromethane / pentane 5:1) afforded the alkylated product as a red-brown, crystalline solid (100 mg, 49%; lit. 82%[S1]).

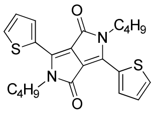

Mp = 165 – 167 °C. ^{1}H NMR (400 MHz, $CDCl_3$, δ/ppm): 8.92 (dd, $^3J = 3.9$ Hz, $^4J = 1.2$ Hz, 2H), 7.63 (dd, $^3J = 5.0$ Hz, $^4J = 1.2$ Hz, 2H), 7.28 (dd, $^3J = 5.0$ Hz, $^3J = 3.9$ Hz, 2H), 4.09 (t, $^3J = 7.8$ Hz, 4H), 1.78 – 1.69 (m, 4H), 1.50 – 1.41 (m, 4H), 0.97 (t, $^3J = 7.4$ Hz, 6H). HRMS (ESI, acetonitrile / chloroform, positive): *m/z*: 412.1272 $[M]^+$, calcd for $C_{22}H_{24}N_2O_2S_2$: 412.1274. Elemental analysis (%): calcd for $C_{22}H_{24}N_2O_2S_2$: C, 64.05; H, 5.86; N, 6.79; S, 15.54; found: C, 64.18; H, 5.99; N, 6.98; S, 15.59. UV/Vis (CH_2Cl_2): λ_{max} / nm (ε / M^{-1} cm^{-1}) = 549 (29700), 511 (24500), 291 (27400).

2,5-Bis(*n*-pentyl)-3,6-bis(thiophen-2-yl)-pyrrolo[3,4-*c*]pyrrole-1,4-dione (H-**DPP**-C_5)

According to the general procedure Th_2-DPP (150 mg, 0.497 mmol), potassium carbonate (274 mg, 2.00 mmol) and *n*-pentyl bromide (0.37 mL, 0.30 mg, 2.0 mmol) were reacted in DMF (11 mL) for 5 h. Column chromatography (dichloromethane / pentane 4:1) yielded a red-brown crystalline solid (84.8 mg, 39%).

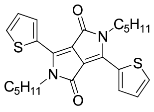

Mp = 176 – 179 °C. ^{1}H NMR (400 MHz, $CDCl_3$, δ/ppm): 8.92 (dd, $^3J = 3.9$ Hz, $^4J = 1.1$ Hz, 2H), 7.63 (dd, $^3J = 5.0$ Hz, $^4J = 1.1$ Hz, 2H), 7.28 (dd, $^3J = 5.0$ Hz, $^3J = 3.9$ Hz, 2H), 4.07 (t, $^3J = 7.9$ Hz, 4H), 1.79 – 1.71 (m, 4H), 1.45 – 1.29 (m, 8H), 0.91 (t, $^3J = 7.1$ Hz, 6H). HRMS (ESI, acetonitrile / chloroform, positive): *m/z:* 441.1666 $[M+H]^+$, calcd for $C_{24}H_{29}N_2O_2S_2$: 441.1665. Elemental analysis (%): calcd for $C_{24}H_{28}N_2O_2S_2$: C, 65.42; H, 6.41; N, 6.36; S, 14.55; found: C, 65.37; H, 6.68; N, 6.49; S, 14.32. UV/Vis (CH_2Cl_2): λ_{max} / nm (ε / M^{-1} cm^{-1}) = 549 (29700), 511 (24600), 291 (27400).

2,5-Bis(*n*-hexyl)-3,6-bis(thiophen-2-yl)-pyrrolo[3,4-*c*]pyrrole-1,4-dione (H-**DPP**-C_6)
According to the general procedure Th_2-DPP (700 mg, 2.32 mmol), potassium carbonate (1.28 g, 9.31 mmol) and *n*-hexyl bromide (1.3 mL, 1.5 g, 9.3 mmol) were reacted in DMF (50 mL) for 18 h. Column chromatography (dichloromethane / pentane 4:1) afforded a red-brown crystalline solid (474 mg, 44%; lit. 64%[S2]).

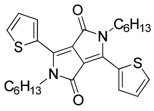

Mp = 177 – 180 °C. ^{1}H NMR (400 MHz, $CDCl_3$, δ/ppm): 8.92 (dd, $^3J = 3.9$ Hz, $^4J = 1.2$ Hz, 2H), 7.63 (dd, $^3J = 5.0$ Hz, $^4J = 1.2$ Hz, 2H), 7.28 (dd, $^3J = 5.0$ Hz, $^3J = 3.9$ Hz, 2H), 4.07 (t, $^3J = 7.9$ Hz, 4H), 1.79 – 1.70 (m, 4H), 1.49 – 1.22 (m, 12H), 0.88 (t, $^3J = 7.1$ Hz, 6H). HRMS (ESI, acetonitrile / chloroform, positive): *m/z*: 469.1979 $[M+H]^+$, calcd for $C_{26}H_{33}N_2O_2S_2$: 469.1978. Elemental analysis (%): calcd for $C_{26}H_{32}N_2O_2S_2$: C, 66.63; H, 6.88; N, 5.98; S, 13.68; found: C, 66.60; H, 6.84; N, 6.15; S, 13.82; UV/Vis (CH_2Cl_2): λ_{max} / nm (ε / M^{-1} cm^{-1}) = 549 (30500), 511 (25000), 291 (27700).

2,5-Bis(*n*-heptyl)-3,6-bis(thiophen-2-yl)-pyrrolo[3,4-*c*]pyrrole-1,4-dione (H-**DPP**-C_7)
According to the general procedure Th_2-DPP (700 mg, 2.32 mmol), potassium carbonate (1.28 g, 9.31 mmol) and *n*-heptyl bromide (1.5 mL, 1.7 g, 9.3 mmol) were reacted in DMF (1.5 mL) for 18 h. Column chromatography (dichloromethane / pentane 3:1) yielded a red-brown crystalline solid (539 mg, 47%).

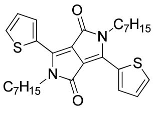

Mp = 145 – 148 °C. ^{1}H NMR (400 MHz, $CDCl_3$, δ/ppm): 8.92 (dd, $^3J = 3.9$ Hz, $^4J = 1.2$ Hz, 2H), 7.63 (dd, $^3J = 5.0$ Hz, $^4J = 1.2$ Hz, 2H), 7.28 (dd, $^3J = 5.0$ Hz, $^3J = 3.9$ Hz, 2H), 4.07 (t, $^3J = 7.9$ Hz, 4H), 1.79 – 1.70 (m, 4H), 1.47 – 1.20 (m, 16H), 0.87 (t, $^3J = 6.9$ Hz, 6H). HRMS (ESI, acetonitrile / chloroform, positive): *m/z*: 496.2216 $[M]^+$, calcd for $C_{28}H_{36}N_2O_2S_2$: 496.2213. Elemental analysis (%): calcd for $C_{28}H_{36}N_2O_2S_2$: C, 67.70; H, 7.30; N, 5.64; S, 12.91; found: C, 67.87; H, 7.30; N, 5.80; S, 13.13. UV/Vis (CH_2Cl_2): λ_{max} / nm (ε / M^{-1} cm^{-1}) = 549 (29700), 511 (24400), 291 (27000).

2,5-Bis(*n*-octyl)-3,6-bis(thiophen-2-yl)-pyrrolo[3,4-*c*]pyrrole-1,4-dione (H-**DPP**-C_8)

According to the general procedure Th_2-DPP (500 mg, 1.67 mmol), potassium carbonate (917 mg, 6.65 mmol) and *n*-octyl bromide (1.2 mL, 1.3 g, 6.7 mmol) were reacted in DMF (35 mL) for 18 h. Column chromatography (dichloromethane / pentane 3:1) yielded a red-brown crystalline solid (415 mg, 48%; lit. 72%[S2]).

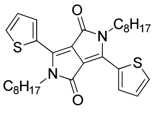

Mp = 142 – 145 °C. ^{1}H NMR (400 MHz, $CDCl_3$, δ/ppm): 8.92 (dd, $^3J = 3.9$ Hz, $^4J = 1.2$ Hz, 2H), 7.63 (dd, $^3J = 5.0$ Hz, $^4J = 1.2$ Hz, 2H), 7.28 (dd, $^3J = 5.0$ Hz, $^3J = 3.9$ Hz, 2H), 4.07 (t, $^3J = 7.9$ Hz, 4H), 1.79 – 1.70 (m, 4H), 1.47 – 1.19 (m, 20H), 0.87 (t, $^3J = 6.9$ Hz, 6H). HRMS (ESI, acetonitrile / chloroform, positive): *m/z:* 524.2525 $[M]^+$, calcd for $C_{30}H_{40}N_2O_2S_2$: 524.2526. Elemental analysis (%): calcd for $C_{30}H_{40}N_2O_2S_2$: C, 68.66; H, 7.68; N, 5.34; S, 12.22; found: C, 68.70; H, 7.70; N, 5.47; S, 12.46. UV/Vis (CH_2Cl_2): λ_{max} / nm (ε / M^{-1} cm^{-1}) = 549 (30400), 511 (24900), 291 (28100). Fluorescence (CH_2Cl_2, $\lambda_{ex} = 516$ nm): $\lambda_{max} = 562$ nm; $\Phi_{Fl} = 100\%$. CV (CH_2Cl_2, 0.1 M TBAHFP, vs. Fc/Fc^+): $E_{1/2}^{Red1} = -1.67$ V, $E_{1/2}^{Ox1} = 0.50$ V, $E_{1/2}^{Ox2} = 0.88$ V.

2,5-Bis(2-ethylhexyl)-3,6-bis(thiophen-2-yl)-pyrrolo[3,4-*c*]pyrrole-1,4-dione

(H-**DPP**-Ethex)

According to the general procedure Th_2-DPP (9.35 g, 31.2 mmol), potassium carbonate (17.3 g, 125 mmol) and 2-ethylhexyl bromide (27.8 g, 144 mmol) were reacted in DMF (180 mL) for 18 h. Column chromatography (dichloromethane) yielded a red-brown crystalline solid (3.8 g, 23%; lit. 41%[S2]).

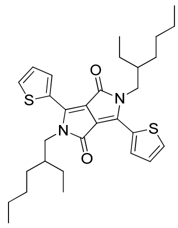

Mp. = 131 – 132 °C. ^{1}H NMR (400 MHz, CD_2Cl_2, δ/ppm): 8.84 (dd, $^3J = 3.9$ Hz, $^4J = 1.2$ Hz, 2H), 7.67 (dd, $^3J = 5.0$ Hz, $^4J = 1.2$ Hz, 2H), 7.29 (dd, $^3J = 5.0$ Hz, $^3J = 3.9$ Hz, 2H), 4.06 – 3.95 (m, 4H), 1.88 – 1.78 (m, 2H), 1.39 – 1.18 (m, 16H), 0.91 – 0.81 (m, 12H). HRMS (ESI, acetonitrile / chloroform, positive): *m/z*: 524.2517 $[M]^+$, calcd for $C_{30}H_{40}N_2O_2S_2$: 524.2526. Elemental analysis (%): calcd for $C_{30}H_{40}N_2O_2S_2$: C, 68.66; H, 7.68; N, 5.34; S, 12.22; found: C, 68.66; H, 7.75; N, 5.39; S, 12.16. UV/Vis (CH_2Cl_2): λ_{max} / nm (ε / M^{-1} cm^{-1}) = 549 (27600), 513 (24600), 292 (22500).

General procedure for the chlorination and bromination:

The synthesis of several brominated DPP derivates by bromination with *N*-bromosuccinimide (NBS) in chloroform was described previously (Br-**DPP**-C4[S1], Br-**DPP**-C6[S3], Br-**DPP**-C8[S2], Br-**DPP**-Ethex[S4]). Following these procedures, the bromination was performed in dichloromethane. The chlorination reactions with *N*-chlorosuccinimide (NCS) as chlorinating agent were performed in dichloromethane as well:

The respective H-DPP derivative and the halogenation reagent were placed in a round-bottomed flask under argon and dry dichloromethane was added. The mixture was stirred at room temperature for the specified time period. The reaction mixture was subjected to column chromatography with dichloromethane / pentane 1:1 as an eluent, unless otherwise noted. The product was then suspended in hexane, filtered and dried under vacuum.

2,5-Bis(*n*-butyl)-3,6-bis(5-chlorothiophen-2-yl)-pyrrolo[3,4-*c*]pyrrole-1,4-dione

(Cl-**DPP**-C_4)

According to the general procedure, the reaction of H-**DPP**-C_4 (120 mg, 0.290 mmol) and *N*-chlorosuccinimide (96.7 mg, 0.727 mmol) in dichloromethane (7.5 mL) for 18 h yielded a dark powder (49.0 mg, 35%).

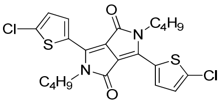

Mp = 251 – 258 °C. ^{1}H NMR (400 MHz, $CDCl_3$, δ/ppm): 8.71 (d, $^3J = 4.2$ Hz, 2H), 7.10 (d, $^3J = 4.2$ Hz, 2H), 3.99 (t, $^3J = 7.8$ Hz, 4H), 1.75 – 1.66 (m, 4H), 1.49 – 1.39 (m, 4H), 0.97 (t, $^3J = 7.3$ Hz, 6H). HRMS (ESI, acetonitrile / chloroform, positive): *m/z:* 480.0493 $[M]^+$, calcd for $C_{22}H_{22}Cl_2N_2O_2S_2$: 480.0494. Elemental analysis (%): calcd for $C_{22}H_{22}Cl_2N_2O_2S_2$: C, 54.88; H, 4.61; N, 5.82; S, 13.32; found: C, 54.83; H, 4.69; N, 5.89; S, 13.26. UV/Vis (CH_2Cl_2): λ_{max} / nm (ε / M^{-1} cm^{-1}) = 565 (33800), 525 (27700), 303 (27900).

2,5-Bis(*n*-pentyl)-3,6-bis(5-chlorothiophen-2-yl)pyrrolo[3,4-*c*]-pyrrole-1,4-dione

(Cl-**DPP**-C_5)

According to the general procedure, the reaction of H-**DPP**-C_5 (527 mg, 1.20 mmol) and *N*-chlorosuccinimide (320 mg, 2.40 mmol) in dichloromethane (250 mL) for 21 h yielded a dark powder (70 mg, 11%). A much higher yield of 51% was obtained in a further experiment on a smaller scale (100 mg H-DPP).

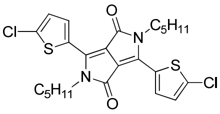

Mp = 239 – 241 °C. ^{1}H NMR (400 MHz, CD_2Cl_2, δ/ppm): 8.70 (d, $^3J = 4.2$ Hz, 2H), 7.14 (d, $^3J = 4.2$ Hz, 2H), 3.98 (t, $^3J = 7.7$ Hz, 4H), 1.74 – 1.66 (m, 4H), 1.43 – 1.24 (m, 8H), 0.91 (t, $^3J = 7.0$ Hz, 6H). HRMS (ESI, acetonitrile / chloroform, positive): *m/z:* 508.0810 $[M]^+$, calcd for $C_{24}H_{26}Cl_2N_2O_2S_2$: 508.0807. Elemental analysis (%): calcd for $C_{24}H_{26}Cl_2N_2O_2S_2$: C, 56.58; H, 5.14; N, 5.50; S, 12.59; found: C, 56.45; H, 5.15; N, 5.44; S, 12.43. UV/Vis (CH_2Cl_2): λ_{max} / nm (ε / M^{-1} cm^{-1}) = 565 (35400), 525 (29000), 303 (29200).

2,5-Bis(*n*-hexyl)-3,6-bis(5-chlorothiophen-2-yl)pyrrolo[3,4-*c*]-pyrrole-1,4-dione (Cl-**DPP**-C$_6$)

According to the general procedure, the reaction of H-**DPP**-C$_6$ (200 mg, 0.427 mmol) and *N*-chlorosuccinimide (143 mg, 1.07 mmol) in dichloromethane (40 mL) for 11 h yielded a dark powder (57 mg, 25%).

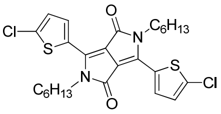

Mp = 231 – 232 °C. ^{1}H NMR (400 MHz, CD_2Cl_2, δ/ppm): 8.69 (d, $^3J = 4.2$ Hz, 2H), 7.14 (d, $^3J = 4.2$ Hz, 2H), 3.97 (t, $^3J = 7.8$ Hz, 4H), 1.74 – 1.64 (m, 4H), 1.42 – 1.30 (m, 12H), 0.89 (t, $^3J = 7.1$ Hz, 6H). HRMS (ESI, acetonitrile / chloroform, positive): *m/z*: 536.1119 [M]$^+$, calcd for $C_{26}H_{30}Cl_2N_2O_2S_2$: 536.1120. Elemental analysis (%):calcd for $C_{26}H_{30}Cl_2N_2O_2S_2$: C, 58.09; H, 5.63; N, 5.21; S, 11.93; calcd for : C, 58.69; H, 5.79; N, 5.36; S, 11.75. UV/Vis (CH_2Cl_2): λ_{max} / nm (ε / M^{-1} cm^{-1}) = 565 (35400), 525 (29000), 303 (29200).

2,5-Bis(*n*-heptyl)-3,6-bis(5-chloro-thiophen-2-yl)pyrrolo[3,4-*c*]-pyrrole-1,4-dione (Cl-**DPP**-C$_7$)

According to the general procedure, the reaction of H-**DPP**-C$_7$ (451 mg, 0.908 mmol) and *N*-chlorosuccinimide (248 mg, 1.86 mmol) in dichloromethane (50 mL) for 25 h yielded a dark powder (165 mg, 32%).

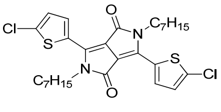

Mp = 209 – 211 °C. ^{1}H NMR (400 MHz, CD_2Cl_2, δ/ppm): 8.70 (d, $^3J = 4.2$ Hz, 2H), 7.14 (d, $^3J = 4.2$ Hz, 2H), 3.97 (t, $^3J = 7.8$ Hz, 4H), 1.74 – 1.66 (m, 4H), 1.43 – 1.24 (m, 16H), 0.88 (t, $^3J = 6.8$ Hz, 6H). HRMS (ESI, acetonitrile / chloroform, positive): *m/z:* 564.1430 [M]$^+$, calcd for $C_{28}H_{34}Cl_2N_2O_2S_2$: 564.1433. Elemental analysis (%): calcd for $C_{28}H_{34}Cl_2N_2O_2S_2$: C, 59.46; H, 6.06; N, 4.95; S, 11.34; found: C, 59.74; H, 6.07; N, 5.16; S, 11.28. UV/Vis (CH_2Cl_2): λ_{max} / nm (ε / M^{-1} cm^{-1}) = 565 (35500), 525 (29200), 303 (29400).

2,5-Bis(*n*-octyl)-3,6-bis(5-chlorothiophen-2-yl)-pyrrolo[3,4-*c*]pyrrole-1,4-dione

(Cl-**DPP**-C_8)

According to the general procedure, the reaction of H-**DPP**-C_8 (140 mg, 0.267 mmol) and *N*-chlorosuccinimide (89.1 mg, 0.667 mmol) in dichloromethane (15 mL) for 18 h and subsequent column chromatography (dichloromethane / pentane 3:5) yielded a dark powder (72.4 mg, 46%).

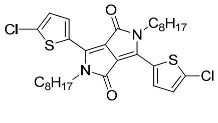

Mp = 200 – 202 °C. ^{1}H NMR (400 MHz, $CDCl_3$, δ/ppm): 8.71 (d, $^3J = 4.2$ Hz, 2H), 7.10 (d, $^3J = 4.2$ Hz, 2H), 3.98 (t, $^3J = 7.8$ Hz, 4H), 1.75 – 1.67 (m, 4H), 1.46 – 1.19 (m, 20H), 0.88 (t, $^3J = 6.9$ Hz, 6H). HRMS (ESI, acetonitrile / chloroform, positive): *m/z:* 592.1748 $[M]^+$, calcd for $C_{30}H_{38}Cl_2N_2O_2S_2$: 592.1746. Elemental analysis (%): calcd for $C_{30}H_{38}Cl_2N_2O_2S_2$: C, 60.69; H, 6.45; N, 4.72; S, 10.80; found: C, 60.68; H, 6.41; N, 4.80; S, 10.72. UV/Vis (CH_2Cl_2): λ_{max} / nm (ε / M^{-1} cm^{-1}) = 565 (35200), 525 (28900), 303 (28900). Fluorescence (CH_2Cl_2, $\lambda_{ex} = 516$ nm): $\lambda_{max} = 578$ nm, $\Phi_{Fl} = 84\%$. CV (CH_2Cl_2, 0.1 M TBAHFP, vs. Fc/Fc^+): $E_{1/2}^{Red1} = -1.57$ V, $E_{1/2}^{Ox1} = 0.55$ V, $E_{1/2}^{Ox2} = 0.88$ V.

2,5-Bis(2-ethylhexyl)-3,6-bis(5-chlorothiophen-2-yl)pyrrolo[3,4-*c*]-pyrrole-1,4-dione

(Cl-**DPP**-Ethex)

A mixture of H-**DPP**-Ethex (1.22 g, 2.33 mmol) and *N*-chlorosuccinimide (635 mg, 4.76 mmol) was stirred in dry dichloromethane (54 mL) at room temperature for 23 h. The solvent was removed under reduced pressure and the residue was purified by column chromatography (dichloromethane / pentane 3:2). The isomeric mixture was dissolved in dichloromethane (175 mL), stored overnight at −20 °C and finally the precipitate was filtered off (611 mg).

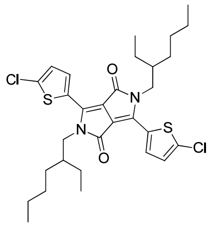

Mp = 171-176 °C. ^{1}H NMR (400 MHz, CD_2Cl_2, δ/ppm): 8.65 (d, ^3J = 4.2 Hz, 2H), 7.12 (d, ^3J = 4.2 Hz, 2H), 4.00 – 3.84 (m, 4H), 1.87-1.76 (m, 2H), 1.40 – 1.18 (m, 16H), 0.91 – 0.83 (m, 12H). HRMS (ESI, acetonitrile / chloroform, positive): *m/z*: 593.1814 $[M+H]^+$, calcd for $C_{30}H_{39}Cl_2N_2O_2S_2$: 593.1825. Elemental analysis (%): calcd for $C_{30}H_{38}Cl_2N_2O_2S_2$: C, 60.70; H, 6.45; N, 4.72; S, 10.80; found C, 60.83; H, 6.47; N, 4.67; S, 10.42. UV/Vis (CH_2Cl_2): λ_{max} / nm (ε / M^{-1} cm^{-1}) = 565 (30600), 525 (27200), 303 (25800).

2,5-Bis(*n*-butyl)-3,6-bis(5-bromothiophen-2-yl)-pyrrolo[3,4-*c*]pyrrole-1,4-dione

(Br-**DPP**-C_4)

According to the general procedure, the reaction of H-**DPP**-C_4 (120 mg, 0.290 mmol) and *N*-bromosuccinimide (129 mg, 0.727 mmol) in dichloromethane (7.5 mL) for 18 h yielded a dark powder (110 mg, 67%; lit. 75% [S1]).

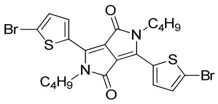

Mp = 260 – 262 °C. ^{1}H NMR (400 MHz, $CDCl_3$, δ/ppm): 8.68 (d, ^3J = 4.2 Hz, 2H), 7.24 (d, ^3J = 4.2 Hz, 2H), 4.00 (t, ^3J = 7.7 Hz, 4H), 1.75 – 1.67 (m, 4H), 1.50 – 1.40 (m, 4H), 0.98 (t, ^3J = 7.3 Hz, 6H). HRMS (ESI, acetonitrile / chloroform, positive): *m/z:* 567.9485 $[M]^+$, calcd for $C_{22}H_{22}Br_2N_2O_2S_2$: 567.9484. Elemental analysis (%): calcd for $C_{22}H_{22}Br_2N_2O_2S_2$: C, 46.33; H, 3.89; N, 4.91; S, 11.24; found: C, 46.64; H, 3.94; N, 4.88; S, 11.02. UV/Vis (CH_2Cl_2): λ_{max} / nm (ε / M^{-1} cm^{-1}) = 568 (36700), 527 (29800), 303 (26600).

2,5-Bis(*n*-pentyl)-3,6-bis(5-bromothiophen-2-yl)-pyrrolo[3,4-*c*]pyrrole-1,4-dione

(Br-**DPP**-C_5)

According to the general procedure, the reaction of H-**DPP**-C_5 (200 mg, 0.380 mmol) and *N*-bromosuccinimide (180 mg, 1.01 mmol) in dichloromethane (10 mL) for 18 h yielded a dark powder (184 mg, 81%).

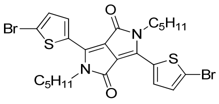

Mp = 246 – 247 °C. ^{1}H NMR (400 MHz, $CDCl_3$, δ/ppm): 8.68 (d, $^3J = 4.2$ Hz, 2H), 7.24 (d, $^3J = 4.2$ Hz, 2H), 3.99 (t, $^3J = 7.8$ Hz, 4H), 1.76 – 1.68 (m, 4H), 1.41 – 1.35 (m, 8H), 0.92 (t, $^3J = 7.0$ Hz, 6H). HRMS (ESI, acetonitrile / chloroform, positive): *m/z:* 595.9793 $[M]^+$, calcd for $C_{24}H_{26}Br_2N_2O_2S_2$: 595.9797. Elemental analysis (%):calcd for $C_{24}H_{26}Br_2N_2O_2S_2$: C, 48.17; H, 4.38; N, 4.68; S, 10.72; found: C, 48.17; H, 4.36; N, 4.81; S, 10.84; UV/Vis (CH_2Cl_2): λ_{max} / nm (ε / M^{-1} cm^{-1}) = 568 (37000), 527 (30000), 303 (26800).

2,5-Bis(*n*-hexyl)-3,6-bis(5-bromothiophen-2-yl)-pyrrolo[3,4-*c*]pyrrole-1,4-dione
(Br-**DPP**-C_6)

According to the general procedure, the reaction of H-**DPP**-C_6 (130 mg, 0.277 mmol) and *N*-bromosuccinimide (123 mg, 0.693 mmol) in dichloromethane (10 mL) for 18 h yielded a dark powder (131 mg, 75%; lit. 65%[S3]).

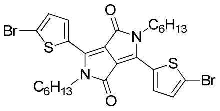

Mp = 231 – 234 °C. ^{1}H NMR (400 MHz, $CDCl_3$, δ/ppm): 8.67 (d, $^3J = 4.2$ Hz, 2H), 7.24 (d, $^3J = 4.2$ Hz, 2H), 3.99 (t, $^3J = 7.8$ Hz, 4H), 1.76 – 1.67 (m, 4H), 1.47 – 1.24 (m, 12H), 0.89 (t, $^3J = 7.0$ Hz, 6H). HRMS (ESI, acetonitrile / chloroform, positive): *m/z*: 624.0119 $[M]^+$, calcd for $C_{26}H_{30}Br_2N_2O_2S_2$: 624.0110. Elemental analysis (%): calcd for $C_{26}H_{30}Br_2N_2O_2S_2$: C, 49.85; H, 4.83; N, 4.47; S, 10.24; found: C, 49.65; H, 4.76; N, 4.62; S, 10.33. UV/Vis (CH_2Cl_2): λ_{max} / nm (ε / M^{-1} cm^{-1}) = 568 (37400), 527 (30400), 304 (27100).

2,5-Bis(*n*-heptyl)-3,6-bis(5-bromothiophen-2-yl)-pyrrolo[3,4-*c*]pyrrole-1,4-dione
(Br-**DPP**-C_7)

A mixture of H-**DPP**-C_7 (1.00 g, 2.01 mmol) and *N*-bromosuccinimide (896 mg, 5.03 mmol) in dichloromethane (65 mL) was stirred at room temperature for 20 h. The reaction solution was concentrated under reduced pressure, methanol was added and the precipitate was separated by filtration to obtain 1.13 g (86%) of a solid. A small portion of this crude product was purified by column chromatography (dichloromethane / pentane 3:5) and subsequently washed with hexane to yield a dark powder, which was used for the characterization. For the subsequent cyanation, the crude product was used without further purification.

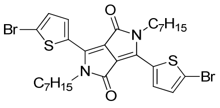

Mp = 213 – 215 °C. ^{1}H NMR (400 MHz, $CDCl_3$, δ/ppm): 8.67 (d, $^3J = 4.2$ Hz, 2H), 7.24 (d, $^3J = 4.2$ Hz, 2H), 3.98 (t, $^3J = 7.8$ Hz, 4H), 1.76 – 1.68 (m, 4H), 1.45 – 1.19 (m, 16H), 0.88 (t, $^3J = 6.9$ Hz, 6H). HRMS (ESI, acetonitrile / chloroform, positive): *m/z*: 653.0500 $[M+H]^+$, calcd for $C_{28}H_{35}Br_2N_2O_2S_2$: 653.0501. Elemental analysis (%): calcd for $C_{28}H_{34}Br_2N_2O_2S_2$: C, 51.38; H, 5.24; N, 4.28; S, 9.80; found: C, 51.55; H, 5.27; N, 4.35; S, 9.42. UV/Vis (CH_2Cl_2): λ_{max} / nm (ε / M^{-1} cm^{-1}) = 568 (36900), 527 (30400), 303 (27000).

2,5-Bis(*n*-octyl)-3,6-bis(5-bromothiophen-2-yl)-pyrrolo[3,4-*c*]pyrrole-1,4-dione

(Br-**DPP**-C_8)

According to the general procedure, the reaction of H-**DPP**-C_8 (130 mg, 0.248 mmol) and *N*-bromosuccinimide (110 mg, 0.619 mmol) in dichloromethane (10 mL) for 40 h and subsequent column chromatography (dichloromethane / pentane 2:3) yielded a dark powder (88.7 mg, 52%; lit. 52%[S2]).

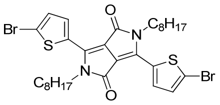

Mp = 202 – 206 °C. ^{1}H NMR (400 MHz, $CDCl_3$, δ/ppm): 8.67 (d, $^3J = 4.2$ Hz, 2H), 7.24 (d, $^3J = 4.2$ Hz, 2H), 3.98 (t, $^3J = 7.8$ Hz, 4H), 1.75 – 1.67 (m, 4H), 1.47 – 1.18 (m, 20H), 0.87 (t, $^3J = 6.9$ Hz, 6H). HRMS (ESI, acetonitrile / chloroform / formic acid, positive): *m/z:* 680.0729 $[M]^+$, calcd for $C_{30}H_{38}Br_2N_2O_2S_2$: 680.0736. Elemental analysis (%): calcd for $C_{30}H_{38}Br_2N_2O_2S_2$: C, 52.79; H, 5.61; N, 4.10; S, 9.40; found: C, 52.76; H, 5.51; N, 4.29; S, 9.39. UV/Vis (CH_2Cl_2): λ_{max} / nm (ε / M^{-1} cm^{-1}) = 568 (37600), 527 (30600), 303 (27200). Fluorescence (CH_2Cl_2, $\lambda_{ex} = 516$ nm): $\lambda_{max} = 580$ nm, Φ_{Fl} = 84%. CV (CH_2Cl_2, 0.1 M TBAHFP, vs. Fc/Fc^+): $E_{1/2}^{Red1} = -1.56$ V, $E_{1/2}^{Ox1} = 0.56$ V, $E_{1/2}^{Ox2} = 0.89$ V.

2,5-Bis(2-ethylhexyl)-3,6-bis(5-bromothiophen-2-yl)pyrrolo[3,4-*c*]-pyrrole-1,4-dione

(Br-**DPP**-Ethex)

A mixture of H-**DPP**- Ethex (2.60 g, 4.95 mmol) and *N*-bromosuccinimide (1.8 g, 10.2 mmol) in dichloromethane (100 mL) was stirred at room temperature for 68 h. The mixture was poured into methanol (120 mL), and the precipitate was filtered off and washed with hot methanol yielding a dark powder (2.19 g, 65%). For the subsequent cyanation the crude product was used without further purification. For the product characterization and use in TFT, a portion of the crude product was purified by column chromatography (dichloromethane / pentane 1:1).

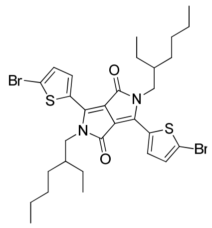

Mp = 166 – 168 °C. ^{1}H NMR (400 MHz, $CDCl_3$, δ/ppm): 8.64 (d, $^3J = 4.2$ Hz, 2H), 7.23 (d, $^3J = 4.2$ Hz, 2H), 4.02 – 3.86 (m, 4H), 1.89 – 1.77 (m, 2H), 1.41 – 1.91 (m, 12H), 0.92 – 0.81 (m, 12H). HRMS (ESI, acetonitrile / chloroform, positive): *m/z*: 680.0723 $[M]^+$, calcd for $C_{30}H_{38}Br_2N_2O_2S_2$: 680.0736. Elemental analysis (%): calcd for $C_{30}H_{38}Br_2N_2O_2S_2$: C, 52.79; H, 5.61; N, 4.10; S, 9.40; found: C, 52.74; H, 5.67; N, 4.19; S, 9.45. UV/Vis (CH_2Cl_2): λ_{max} / nm (ε / M^{-1} cm^{-1}) = 567 (34200), 527 (30000), 304 (35400).

General procedure for DPP cyanation

The respective Br-DPP derivative and copper(I) cyanide were heated in dry DMF at specified temperature for a particular time period under an argon atmosphere. The solvent was removed under reduced pressure and the resulting solid was purified by Soxhlet extraction using chloroform. The chloroform phase was concentrated, subjected to column chromatography (dichloromethane) and the product washed with hexane.

2,5-Bis(*n*-butyl)-3,6-bis(5-cyanothiophen-2-yl)-pyrrolo[3,4-*c*]pyrrole-1,4-dione

(CN-**DPP**-C_4)

According to the general procedure, the reaction of compound Br-**DPP**-C_4 (1.08 g, 1.89 mmol) and copper(I) cyanide (4.00 g, 44.6 mmol) in dry DMF (15 mL) at 130 °C for 315 min and at 165 °C for 40 min afforded a dark violet solid (333 mg, 38%).

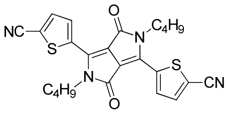

Mp = 287 – 288 °C. ^{1}H NMR (400 MHz, CD_2Cl_2, δ/ppm): 8.87 (d, ^3J = 4.2 Hz, 2H), 7.77 (d, ^3J = 4.2 Hz, 2H), 4.04 (t, ^3J = 7.6 Hz, 4H), 1.74 – 1.64 (m, 4H), 1.49 – 1.38 (m, 4H), 0.97 (t, ^3J = 7.4 Hz; 6H). HRMS (ESI, acetonitrile / chloroform, positive): *m/z:* 463.1256 $[M+H]^+$, calcd for $C_{24}H_{23}N_4O_2S_2$: 463.1257. Elemental analysis (%): calcd for $C_{24}H_{22}N_4O_2S_2$: C, 62.31; H, 4.79; N, 12.11; S, 13.86; found: C, 62.32; H, 4.82; N, 12.05; S, 13.94; λ_{max} / nm (ε / M^{-1} cm^{-1}) = 586 (30720), 545 (26900), 307 (36200).

2,5-Bis(*n*-pentyl)-3,6-bis(5-cyanothiophen-2-yl)-pyrrolo[3,4-*c*]pyrrole-1,4-dione
(CN-**DPP**-C_5)

According to the general procedure, the reaction of compound Br-**DPP**-C_5 (600 mg, 1.00 mmol) and copper(I) cyanide (1.60 g, 18.0 mmol) in dry DMF (15 mL) at 120 °C for 1 h and at 165 °C for 80 min afforded a dark violet solid (64.0 mg, 13%).

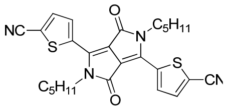

Mp = 273 – 274 °C. ^{1}H NMR (400 MHz, CD_2Cl_2, δ/ppm): 8.87 (d, ^3J = 4.2 Hz, 2H), 7.77 (d, ^3J = 4.2 Hz, 2H), 4.03 (t, ^3J = 7.8 Hz, 4H), 1.75 – 1.66 (m, 4H), 1.44 – 1.34 (m, 8H), 0.92 (t, ^3J = 7.1 Hz; 6H). HRMS (ESI, acetonitrile / chloroform, positive): *m/z:* 491.1568 $[M+H]^+$, calcd for $C_{26}H_{27}N_4O_2S_2$: 491.1570. Elemental analysis (%): calcd for $C_{26}H_{26}N_4O_2S_2$ C, 63.65; H, 5.34; N, 11.42; S, 13.07; found: C, 63.57; H, 5.23; N, 11.38; S, 13.05. UV/Vis (CH_2Cl_2): λ_{max} / nm (ε / M^{-1} cm^{-1}) = 586 (30000), 545 (26300), 307 (35000).

2,5-Bis(*n*-hexyl)-3,6-bis(5-cyanothiophen-2-yl)-pyrrolo[3,4-*c*]pyrrole-1,4-dione
(CN-**DPP**-C_6)

According to the general procedure, the reaction of compound Br-**DPP**-C_6 (237 mg, 0.378 mmol) and copper(I) cyanide (1.50 g, 17.0 mmol) in dry DMF (10 mL) at 130 °C for 4 h afforded a dark violet solid (52 mg, 27%).

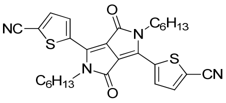

Mp = 251 – 253 °C. ^{1}H NMR (400 MHz, CD_2Cl_2, δ/ppm): 8.86 (d, $^3J = 4.2$ Hz, 2H), 7.77 (d, $^3J = 4.2$ Hz, 2H), 4.03 (t, $^3J = 7.8$ Hz, 4H), 1.75 – 1.65 (m, 4H), 1.46 – 1.27 (m, 12H), 0.90 (t, $^3J = 7.1$ Hz, 6H). HRMS (ESI, acetonitrile / chloroform, positive): *m/z:* 518.1807 $[M]^+$, calcd for $C_{28}H_{30}N_4O_2S_2$: 518.1805. Elemental analysis (%): calcd for $C_{28}H_{30}N_4O_2S_2$: C, 64.84; H, 5.83; N, 10.80; S, 12.36; found: C, 64.69; H, 5.69; N, 10.81, S, 12.50. UV/Vis (CH_2Cl_2): λ_{max} / nm (ε / M^{-1} cm^{-1}) = 586 (31800), 545 (27700), 307 (36700). CV (CH_2Cl_2, 0.1 M TBAHFP, vs. Fc/Fc$^+$): $E_{1/2}^{Red2} = -1.73$ V $E_{1/2}^{Red1} = -1.22$ V, $E_{1/2}^{Ox} = 0.83$ V.

2,5-Bis(*n*-heptyl)-3,6-bis(5-cyanothiophen-2-yl)-pyrrolo[3,4-*c*]pyrrole-1,4-dione

(CN-**DPP**-C_7)

According to the general procedure, the reaction of compound Br-**DPP**-C_7 (1.09 g, 1.67 mmol) and copper(I) cyanide (3.30 g, 36.9 mmol) in dry DMF (40 mL) at 160 °C for 3.5 h afforded a dark violet solid (426 mg, 47%).

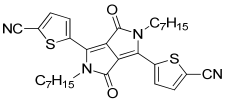

Mp = 228 – 229 °C. ^{1}H NMR (400 MHz, CD_2Cl_2, δ/ppm): 8.86 (d, $^3J = 4.2$ Hz, 2H), 7.77 (d, $^3J = 4.2$ Hz, 2H), 4.03 (t, $^3J = 7.7$ Hz, 4H), 1.74 – 1.64 (m, 4H), 1.45 – 1.25 (m, 16H), 0.88 (t, $^3J = 6.9$ Hz, 6H). HRMS (ESI, acetonitrile / chloroform, positive): *m/z:* 547.2193 $[M+H]^+$, calcd for : $C_{30}H_{35}N_4O_2S_2$: 547.2196. Elemental analysis (%): calcd for $C_{30}H_{34}N_4O_2S_2$: C, 65.90; H, 6.27; N, 10.25; S, 11.73; found: C, 65.90; H, 6.45; N, 10.11; S, 11.88. UV/Vis (CH_2Cl_2): λ_{max} / nm (ε / M^{-1} cm^{-1}) = 586 (32000), 545 (27900), 307 (36800).

2,5-Bis(*n*-octyl)-3,6-bis(5-cyanothiophen-2-yl)-pyrrolo[3,4-*c*]pyrrole-1,4-dione

(CN-**DPP**-C_8)

According to the general procedure, the reaction of compound Br-**DPP**-C_8 (483 mg, 0.708 mmol) and copper(I) cyanide (1.40 g, 15.6 mmol) in dry DMF (10 mL) at 160 °C for 60 min afforded a dark violet solid (96.5 mg, 24%).

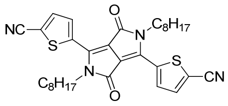

Mp = 226 – 227 °C. ^{1}H NMR (400 MHz, CD_2Cl_2, δ/ppm): 8.90 (d, $^3J = 4.2$ Hz, 2H), 7.75 (d, $^3J = 4.2$ Hz, 2H), 4.03 (t, $^3J = 7.8$ Hz, 4H), 1.75 – 1.68 (m, 4H), 1.46 – 1.20 (m, 20H), 0.88 (t, $^3J = 6.9$ Hz; 6H). HRMS (ESI, acetonitrile / chloroform, positive): *m/z:* 575.2511 $[M+H]^+$, calcd for $C_{32}H_{39}N_4O_2S_2$: 575.2509. Elemental analysis (%): calcd for $C_{32}H_{38}N_4O_2S_2$: C, 66.87; H, 6.66; N, 9.75; O, 5.57; S, 11.16; found: C, 66.67; H, 6.71; N, 9.60; S, 11.09. UV/Vis (CH_2Cl_2): λ_{max} / nm (ε / M^{-1} cm^{-1}) = 586 (31500), 545 (27400), 307 (36200). Fluorescence (CH_2Cl_2, λ_{ex} = 516 nm): λ_{max} = 609 nm, Φ_{Fl} = 70%. CV (CH_2Cl_2, 0.1 M TBAHFP, vs. Fc/Fc^+): $E_{1/2}^{Red2} = -1.75$ V, $E_{1/2}^{Red1} = -1.23$ V, $E_{1/2}^{Ox1} = 0.83$ V.

2,5-Bis(2-ethylhexyl)-3,6-bis(5-cyanothiophen-2-yl)pyrrolo[3,4-*c*]-pyrrole-1,4-dione
(CN-**DPP**-Ethex)

CN-**DPP**-Ethex was prepared according to the previously described literature procedure. [S5]

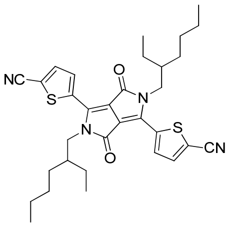

Mp = 223 – 225 °C. ^{1}H NMR (400 MHz, CD_2Cl_2, δ/ppm): 8.82 (d, $^3J = 4.2$ Hz, 2H), 7.76 (d, $^3J = 4.2$ Hz, 2H), 4.03 – 3.91 (m, 4H), 1.84 – 1.72 (m, 2H), 1.40 – 1.18 (m, 16H), 0.91 – 0.82 (m, 12H). ^{13}C NMR (101 MHz, CD_2Cl_2): 161.5, 139.8, 138.3, 135.7, 134.8, 113.9, 113.7, 110.9, 46.4, 39.7, 30.5, 28.7, 23.9, 23,4, 14.2, 10.5. HRMS (ESI, acetonitrile / chloroform, positive): *m/z* 575.2510 $[M+H]^+$, calcd for $C_{32}H_{39}N_4O_2S_2$: 575.2510. Elemental analysis (%): calcd for $C_{32}H_{38}N_4O_2S_2$: C, 66.87; H, 6.66; N, 9.75; S, 11.16; found C, 66.60; H, 6.62; N, 9.77; S, 11.09. UV/Vis (CH_2Cl_2): λ_{max} / nm (ε / M^{-1} cm^{-1}) = 586 (28500), 546 (26500), 308 (34200). CV (CH_2Cl_2, 0.1 M TBAHFP, vs. Fc/Fc^+): $E_{1/2}^{Red2} = -1.77$ V, $E_{1/2}^{Red1} = -1.24$ V, $E_{1/2}^{Ox1} = 0.86$ V.

Table S1. Optical properties of compounds X-**DPP**-C_n/Ethex (X: H, Cl, Br, CN; n = 4-8) at a concentration of 10^{-5} M in CH_2Cl_2 at 298 K.

DPP	R	λ_{max} [nm] (ε_{max} [M^{-1} cm^{-1}])	E_{hv} [eV]
H-**DPP**-R	C_4	549 (29700), 511 (24500)	2.26
	C_5	549 (29700), 511 (24600)	2.26
	C_6	549 (30500), 511 (25000)	2.26
	C_7	549 (29700), 511 (24400)	2.26
	C_8	549 (30400), 511 (24900)	2.26
	Ethex	549 (27600), 513 (24600)	2.26
Cl-**DPP**-R	C_4	565 (33800), 525 (27700)	2.19
	C_5	565 (35400), 525 (29000)	2.19
	C_6	565 (35400), 525 (29000)	2.19
	C_7	565 (35500), 525 (29200)	2.19
	C_8	565 (35200), 525 (28900)	2.19
	Ethex	565 (30600), 525 (27200)	2.19
Br-**DPP**-R	C_4	568 (36700), 527 (29800)	2.18
	C_5	568 (37000), 527 (30000)	2.18
	C_6	568 (37400), 527 (30400)	2.18
	C_7	568 (36900), 527 (30400)	2.18
	C_8	568 (37600), 527 (30600)	2.18
	Ethex	567 (34200), 527 (30000)	2.18
CN-**DPP**-R	C_4	586 (30720), 545 (26900)	2.12
	C_5	586 (30000), 545 (26300)	2.12
	C_6	586 (31800), 545 (27700)	2.12
	C_7	586 (32000), 545 (27900)	2.12
	C_8	586 (31500), 545 (27400)	2.12
	Ethex	586 (28500), 546 (26500)	2.12

2. TFT Measurements

Table S2. Hole mobility (μ_p), threshold voltage (V_T) and on/off current ratio (I_{on}/I_{off}) of p-channel TFTs fabricated using compounds X-**DPP**-C$_n$/Ethex (X: H, Cl, Br, CN; n = 4-8). The TFTs were fabricated on doped silicon substrates using an SiO$_2$/Al$_2$O$_3$ gate dielectric functionalized with a fluoroalkylphosphonic acid self-assembled monolayer (SAM). The organic semiconductor films were deposited by sublimation in vacuum (10^{-6} mbar), with the substrate held at an elevated temperature (T_S). The electrical measurements were performed in ambient air at room temperature.

DPP	R	μ_p[a] [cm^2 V^{-1} s^{-1}]	V_T [V]	I_{on}/I_{off} [1]	T_S [°C]
H-**DPP**-R	C$_4$	0.011	2	1 x 10^5	25
	C$_5$	0.011	–2	3 x 10^4	25
	C$_6$	0.010	5	2 x 10^6	25
	C$_7$	0.016	6	8 x 10^4	25
	C$_8$	0.018	9	1 x 10^5	25
	Ethex	0.090	5	1 x 10^7	50
Cl-**DPP**-R	C$_4$	0.06	–4	3 x 10^5	50
	C$_5$	0.08	3	5 x 10^5	70
	C$_6$	0.05	4	5 x 10^5	80
	C$_7$	0.07	3	1 x 10^6	80
	C$_8$	0.06	5	1 x 10^6	70
	Ethex	0.15	6	2 x 10^6	70
Br-**DPP**-R	C$_4$	0.05	–4	2 x 10^5	50
	C$_5$	0.07	–3	2 x 10^5	70
	C$_6$	0.05	5	3 x 10^5	80
	C$_7$	0.06	3	3 x 10^5	80
	C$_8$	0.06	9	2 x 10^5	90
	Ethex	0.12	3	1 x 10^6	70
CN-**DPP**-R	C$_4$	0.015	–14	1 x 10^5	70
	C$_5$	0.40	–15	1 x 10^5	70
	C$_6$	0.04	–16	1 x 10^5	80
	C$_7$	0.02	–15	1 x 10^5	80
	C$_8$	0.03	–16	1 x 10^5	90
	Ethex	0.70	–27	1 x 10^6	70

[a] Average value of five transistors, which showed a variation of less than 10 %.

Table S3. Electron mobility (μ_n), threshold voltage (V_T) and on/off current ratio (I_{on}/I_{off}) of n-channel TFTs fabricated using compounds CN-**DPP**-C_n (n = 4-8). The TFTs were fabricated on doped silicon substrates using a SiO_2/Al_2O_3 gate dielectric functionalized with an alkylphosphonic acid SAM. The organic semiconductor films were deposited by sublimation in vacuum (10^{-6} mbar), with the substrate held at an elevated temperature (T_S). The electrical measurements were performed in ambient air at room temperature.

DPP	C_n	μ_n[a] [$cm^2\ V^{-1}\ s^{-1}$]	V_T [V]	I_{on}/I_{off} [1]	T_S [°C]
CN-**DPP**-C_n	C_4	0.01	15	3×10^5	70
	C_5	0.01	18	2×10^5	70
	C_6	0.04	18	1×10^5	80
	C_7	0.005	25	5×10^4	80
	C_8	0.005	18	1×10^5	90

[a] Average value of five transistors, which showed a variation of less than 10 %.

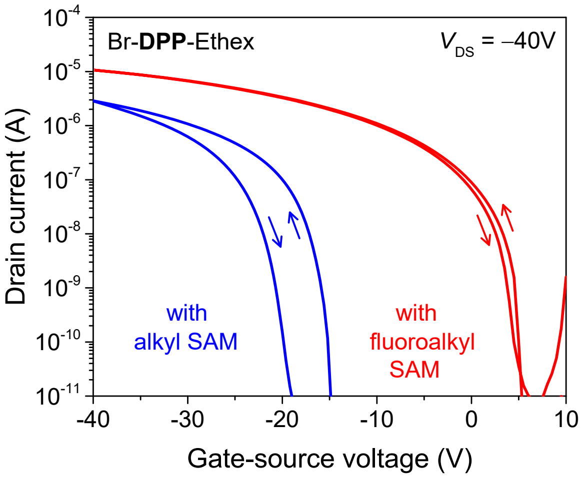

Figure S1. Transfer characteristics of p-channel TFTs based on vacuum-deposited layers of Br-**DPP**-Ethex and either a fluoroalkylphosphonic acid SAM (red) or an alkylphosphonic acid SAM (blue) measured in ambient air. For all the semiconductors investigated here, the TFTs with the alkyl SAM were found to have a large negative threshold voltage, whereas the threshold voltage of the TFTs with the fluoroalkyl SAM is usually close to zero. Also, the TFTs with the fluoroalkyl SAM tend to have a smaller hysteresis in the transfer characteristics than the TFTs with the alkyl SAM. For these reasons, Table S2 is limited to the TFTs with the fluoroalkyl SAM.

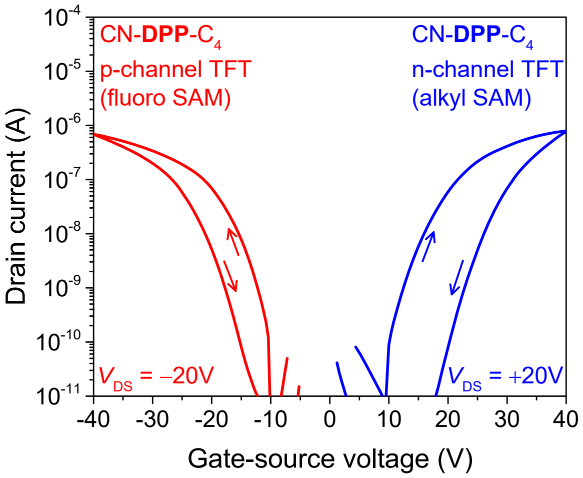

Figure S2. Transfer characteristics of p-channel and n-channel TFTs based on vacuum-deposited layers of CN-**DPP**-C_4 and either a fluoroalkylphosphonic acid SAM (red) or an alkylphosphonic acid SAM (blue) measured in ambient air.

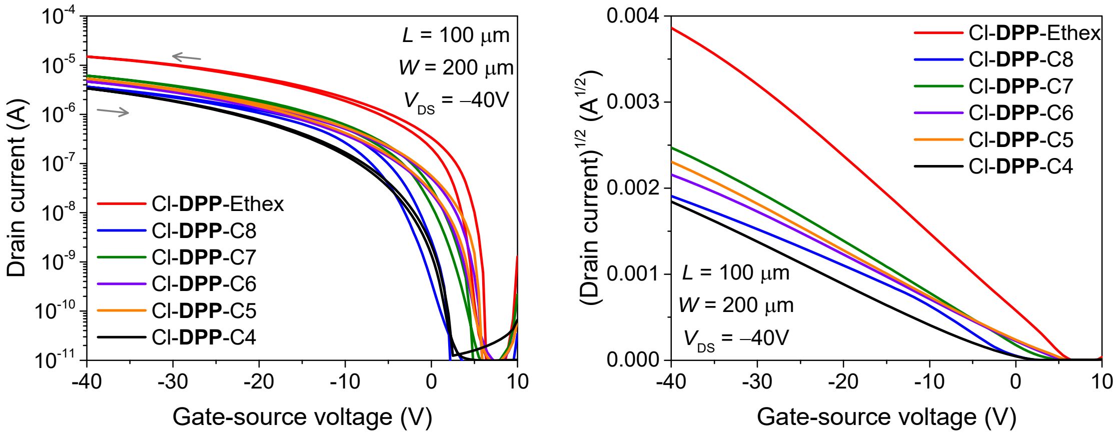

Figure S3. Transfer characteristics of p-channel TFTs based on vacuum-deposited layers of Cl-**DPP**-C_4 (black), Cl-**DPP**-C_5 (orange), Cl-**DPP**-C_6 (violet), Cl-**DPP**-C_7 (green), Cl-**DPP**-C_8 (blue) and Cl-**DPP**-Ethex (red) on a fluoroalkylphosphonic acid SAM.

3. HPLC Analysis

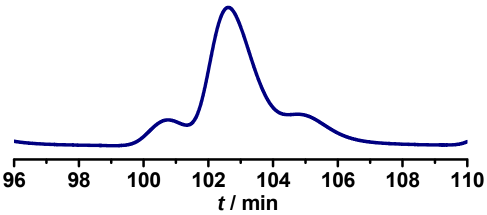

Figure S4. Elution profile from a HPLC equipped with a chiral column of as-synthesized Cl-**DPP**-Ethex after precipitation from a dichloromethane solution upon cooling revealing an about 10:80:10 ratio of (*R*,*R*), (*R*,*S*/*S*,*R*) and (*S*,*S*) stereoisomers.

4. X-ray Crystallography

Table S4. Overview for the crystal structure and refinement data for dyes Cl-DPP-C_n/Ethex (n = 7,8).

	Cl-**DPP**-C_7	Cl-**DPP**-C_8	Cl-**DPP**-Ethex
Chemical formula	$C_{28}H_{34}Cl_2N_2O_2S_2$	$C_{30}H_{38}Cl_2N_2O_2S_2$	$C_{30}H_{38}Cl_2N_2O_2S_2$
Molecular weight [g mol^{-1}]	565.61	593.67	593.67
Temperature [K]	303(2)	295(2)	298(2)
Radiation, λ [Å]	$Cu_{K\alpha}$, 1.54178	$Cu_{K\alpha}$, 1.54178	$Cu_{K\alpha}$, 1.54178
Description of the crystal			
Dimension of the crystal [mm x mm x mm]	0.366 x 0.045 x 0.027	0.520 x 0.0032 x 0.030	0.512 x 0.083 x 0.026
Color	red	red	red
Description	plate	needle	plate
Crystal system	Triclinic	Triclinic	Triclinic
Space group	P–1	P–1	P–1
Dimensions of the unit cell			
a [Å]	4.83360(10)	4.8304(8)	6.5747(4)
b [Å]	8.7496(2)	8.6559(12)	7.8394(5)
c [Å]	17.0825(5)	18.494(3)	14.9616(10)
α [°]	79.9598(11)	80.420(7)	100.785(3)
β [°]	87.6044(12)	87.703(15)	100.795(3)
γ [°]	87.8500(13)	87.368(11)	90.027(3)
Volume [Å^3]	710.43(3)	761.3(2)	743.62(8)
Z	1	1	1
ρ_{calc} [g cm^{-3}]	1.322	1.295	1.326
F(000)	298	314	314
Range of θ [°] cell	2.63 - 74.55	4.85 - 73.98	3.06 - 74.55
Goodness-of-fit for F^2	1.052	1.056	1.063
CCDC	1484925	1484924	1484923

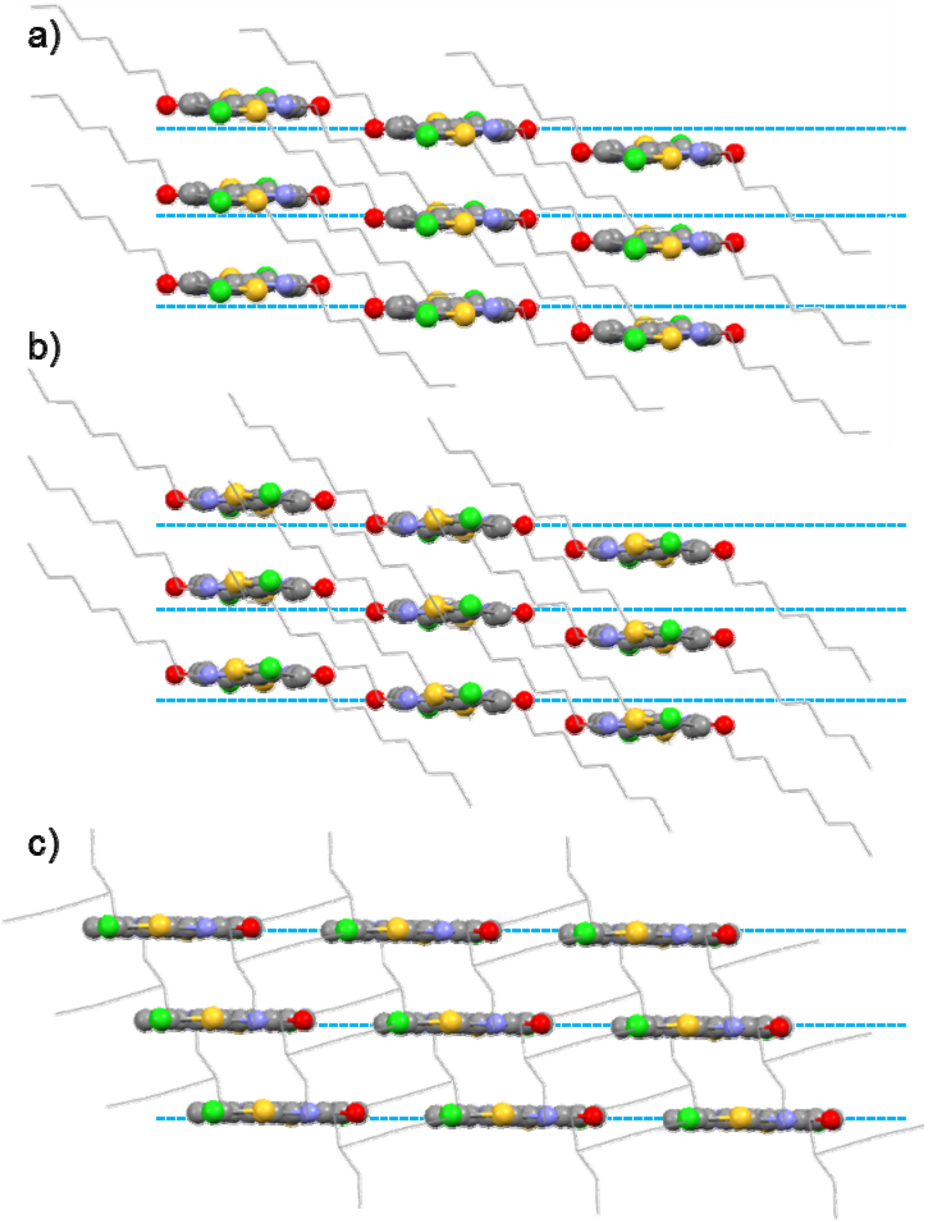

Figure S5. Side view onto the H-bonded staircase-like layers of a) Cl-**DPP**-C_7 and b) Cl-**DPP**-C_8 as well as planar layers of c) Cl-**DPP**-Ethex. Alkyl chains are illustrated in wireframe and each respective layer is indicated by a light blue dashed line.

5. Calculations of the transfer integrals

Calculations of the transfer integrals were done by a fragment orbital approach[S6] and a basis set orthogonalization procedure[S7] with the ADF (Amsterdam density functional) package[S8] using the B3LYP functional[S9] and the TZP basis set.

Table S5. Calculated transfer integrals t_+ between π-stacked and hydrogen-bonded neighbouring molecule within the single crystal structure of Cl-**DPP**-C_7 and Cl-**DPP**-Ethex.

Next neighbour	$\lvert t_+ \rvert$ (Cl-**DPP**-C_7) / meV	$\lvert t_+ \rvert$ (Cl-**DPP**-Ethex) / meV
π-stacked	117	74
hydrogen-bonded	6	11

6. AFM Measurements

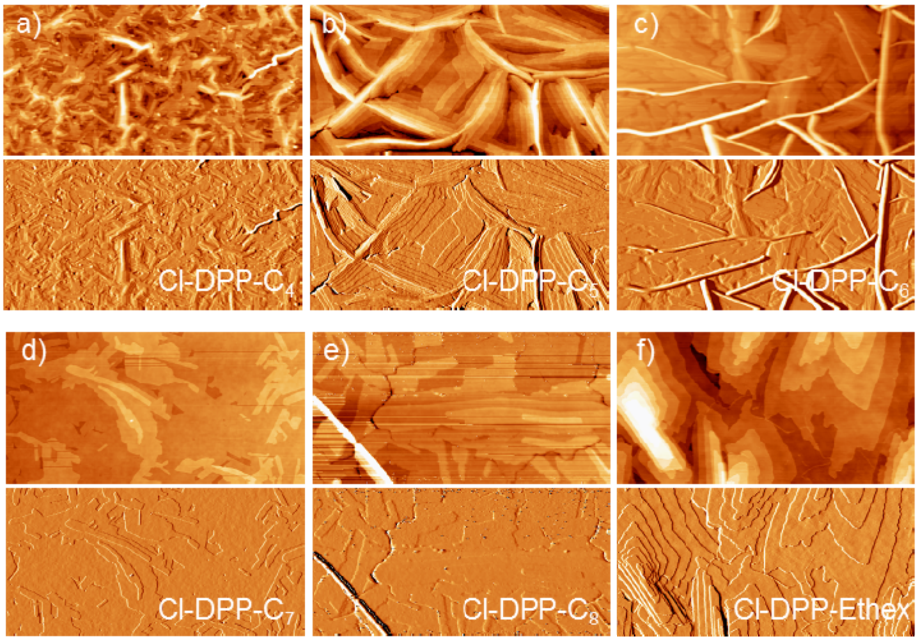

Figure S6. AFM topography (upper panel) and amplitude (lower panel) images of thin layers of compounds Cl-**DPP**-C$_n$/Ethex (n = 4-8) deposited in vacuum onto a fluoroalkylphosphonic acid SAM. During the deposition, the substrate was held at an elevated temperature to promote molecular ordering. The images have an area of 5 µm × 5 µm.

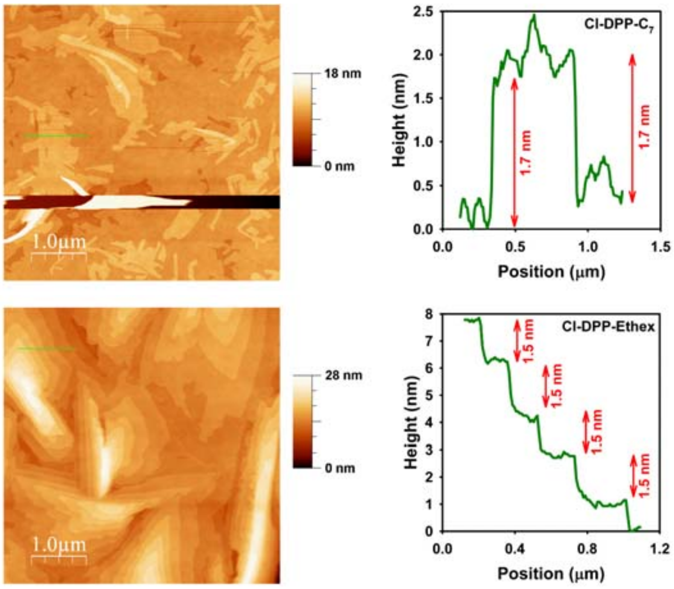

Figure S7. AFM topography images and height profiles of thin layers of Cl-**DPP**-C$_7$ (top) and Cl-**DPP**-Ethex (bottom) deposited in vacuum onto a fluoroalkylphosphonic acid SAM.

7. Additional References

[S1] E. Zhou, Q. Wei, S. Yamakawa, Y. Zhang, K. Tajima, C. Yang, K. Hashimoto, *Macromolecules* **2010**, *43*, 821.

[S2] A. B. Tamayo, M. Tantiwiwat, B. Walker, T.-Q. Nguyen, *J. Phys. Chem. C* **2008**, *112*, 15543.

[S3] C. Kanimozhi, P. Balraju, G. D. Sharma, S. Patil, *J. Phys. Chem. B* **2010**, *114*, 3095.

[S4] L. Huo, J. Hou, H.-Y. Chen, S. Zhang, Y. Jiang, T. L. Chen, Y. Yang, *Macromolecules* **2009**, *42*, 6564.

[S5] S.-L. Suraru, U. Zschieschang, H. Klauk, F. Würthner, *Chem. Commun.* **2011**, *47*, 11504.

[S6] K. Senthilkumar, F. C. Grozema, F. M. Bickelhaupt and L. D. A. Siebbeles, *J. Chem. Phys.,* **2003**, *119*, 9809.

[S7] E. F. Valeev, V. Coropceanu, D. A. da Silva Filho, S. Salman and J.-L. Brédas, *J. Am. Chem. Soc.*, **2006**, *128*, 9882.

[S8] ADF, 2013.01, *Scientific Computing and Modelling NV*, Amsterdam, **2013**.

[S9] (a) A. D. Becke, *Phys. Rev. A*: *At., Mol., Opt. Phys.,* **1988**, *38*, 3098; (b) A. D. Becke, *J. Chem. Phys.*, **1993**, *98*, 5648; (c) C. Lee, W. Yang and R. G. Parr, *Phys. Rev. B: Condens. Matter Mater. Phys.*, **1988**, *37*, 785.